The University of Adelaide

# Age and Basin Evolution of the Cuddapah Supergroup, India

Julie Mackintosh

a1161956
October 2010

# Table of Contents

**Age and Basin Evolution of the Cuddapah Supergroup, India**

*Julie Mackintosh*

Centre for Tectonics, Resources and Exploration

School of Earth and Environmental Sciences

The University of Adelaide, South Australia

# Abstract

U-Pb zircon geochronology indicates deposition of the Cuddapah Supergroup, Cuddapah Basin, India occurred for at least 986 million years. Deposition started after 2502±17 Ma with the deposition of the Gulcheru Formation and ended after 913±11 Ma with the deposition of the Cumbum Formation. Maximum depositional ages have been found for individual formations within the Cuddapah Supergroup; the Pulivendla Formation has a maximum deposition of 1899±19 Ma and the Bairenkonda Formation has a maximum depositional age of 1660±22 Ma. Thermal events during the Palaeoproterozoic present a possible cause of basin formation. At this early stage of the Cuddapah Basin's evolution the provenance of sediments was the Dharwar Craton, which currently underlies the basin and borders it on the north, south and west sides. The uplift of the Eastern Ghats on the eastern margin affected the evolution of the Cuddapah Basin, changing the shape and the sediments of the basin. Uplift and deformation events in the Eastern Ghats folded the eastern side of the Cuddapah Basin and are responsible for its present crescent shape. The formation of the Eastern Ghats caused increased subsidence to the east, creating an asymmetry in the depth of the basin. The provenance of the sediments of the Cuddapah Supergroup changed to the Eastern Ghats for the deposition of the youngest stratigraphic group, the Nallamalai Group.

# Introduction

The Cuddapah Basin of Andhra Pradesh, India, is a crescent shaped Proterozoic intracratonic (Fig. 1) basin nonconformably overlying the Archaean Dharwar Craton. It covers an area of approximately 44500 km$^2$ (Dasgupta *et al.* 2005) and is one of the largest intracratonic basins in India (French *et al.* 2008). The Cuddapah Basin is bordered by the Eastern Ghats Belt, a highly deformed orogenic belt that has been metamorphosed to high grade (Saha 2002, Singh & Mishra 2002), along the eastern margin and bordered by the Dharwar Craton on all other sides. An easterly dipping thrust fault along the eastern margin of the Cuddapah Basin thrusts metamorphic rocks of the Eastern Ghats over the sediments of the Cuddapah Basin (Meijerink *et al.* 1984, Singh & Mishra 2002). The Cuddapah Basin is separated into two sequences; the older Cuddapah Supergroup and the younger Kurnool Group which have been attributed to the Proterozoic (Manikyamba *et al.* 2008). The Cuddapah Supergroup consists predominantly of clastic and chemical sedimentary rocks with minor intercalations of alkali to sub-alkali basaltic flows, mafic/ultramafic sills and ashfall tuffs in the lower part of the succession (French *et al.* 2008).

The basin is divided into sub-basins (Fig. 1) representing the main stratigraphic groups (Fig. 2). The Cuddapah Supergroup is divided in four sequences separated by unconformities (King, 1872, Murphy, 1979), namely the Papaghni, Chitrayati and Nallamalai Groups and the Srisailam Formation (from oldest deposited to youngest). The Srisailam Formation does not crop out in the study area observed and for the purposes of this study is assumed to be equivalent to the Kurnool Group, that overlies the Cuddapah Supergroup. The Papaghni Group consists of the Gulcheru and

Vempalle Formations, the Chitrayati Group consists of the Pulivendla, Tadpatri and Gandikota Formations and the Nallamalai Group consists of the Bairenkonda and Cumbum Formations. The unconformable relationships between the lithostratic groups suggest a history of multiple stages of deposition and erosion.

Although the Cuddapah Basin is accepted by some authors as a foreland basin to the Eastern Ghats orogen (Dasgupta & Biswas 2006, Manikyamba *et al.* 2008) due largely to its shape and location adjacent to the Eastern Ghats the formation of the basin is still a contentious subject. Chaudhuri *et al.* (2002) proposed an alternative model; that the Cuddapah Basin and other intracratonic basins in India developed in rift settings. This theory is based on the existence of deep faults within the Cuddapah Basin exposed by gravity data (NGRI, 1975). Chaudhuri *et al.* (2002) suggest the initial rifts may have followed pre-existing lineaments defined by either Archaean greenstone belts of the Dharwar Craton, or belts of crustal convergence. Hou *et al.* (2008) also suggest it was a rift-type basin formed during the breakup of the Proterozoic Columbia supercontinent.

To better understand what caused the formation of the Cuddapah Basin more evidence is needed on the provenance of the sediments and the tectonic setting at the initiation of the basin. Knowing the time of deposition is essential in finding this evidence. The depositional age of the Cuddapah Basin is not currently well constrained. Sills and carbonates of the Vempalle and Tadpatri Formations have been dated, providing minimum ages for carbonate sedimentation and minimum depositional ages for formations below the sills; 1899±20 Ma. (French *et al.* 2008) is the earliest reported minimum depositional age for the Tadpatri Formation. However, there have been no

robust geochronological studies on the depositional ages of the full sequence of sediments, despite the ~12 km thickness of unmetamorphosed sedimentary rocks preserved. This is the first study to use U-Pb dating techniques to find maximum depositional age constraints on sedimentation.

This study uses LA-ICPMS dating of detrital zircons, Hf isotopes, stable isotope analysis and sequence stratigraphy to investigate the sedimentary evolution and chronostratigraphy of the Cuddapah Supergroup. U-Pb dating of detrital zircons is used to find maximum depositional ages, constraining the timing of deposition. Hf isotope analysis of detrital zircons will be used with U-Pb data to further constrain the source or sources of the sediments by indicating whether the source region is juvenile or not. Sequence stratigraphy is used to determine how the depositional environment changed during the evolution of the basin. An original E-W geological cross-section across the Cuddapah Basin is presented and is used to discuss the structural evolution of the basin. The petroleum potential of the Cuddapah Basin will be briefly discussed using the new knowledge gained by this study of the history of the basin.

# Geological Setting

*Dharwar Craton*

The Cuddapah Supergroup unconformably overlies the Archaean Dharwar Craton (French *et al.* 2008). The Dharwar Craton comprises three main terranes, from west to east; 1) an early to middle Archaean (3400–3000 Ma) tonalitic–trondhjemitic–granodioritic basement (Jayananda *et al.* 2000); 2) volcano-sedimentary greenstone

belts including an older 3580–3200 Ma Sargur Group and a younger 3000–2500 Ma Dharwar Supergroup (Chadwick *et al.* 2000), (Jayananda *et al.* 2000); and 3) late Archaean (2600–2500Ma) calc-alkaline to potassium rich granitic intrusions interspersed with schist belts similar to those of the Dharwar Supergroup (Chadwick *et al.* 2000). These dominate the eastern part of the Dharwar Craton and form the latest magmatic event in the craton (Jayananda *et al.* 2000). Pandey *et al.* (1997) presented Sm-Nd, Rb-Sr and Pb-Pb isotopic data from mafic dykes that suggests a mafic dyke swarm, the Mahbubnagar swarm, was emplaced at ~ 2170 Ma. French *et al.* (2008) dated mafic dykes and sills from the Bastar and Dharwar Cratons; from these results they proposed the existence of a previously unrecognised 1900 Ma large igneous province spanning the Bastar Craton, the Dharwar Craton and the Cuddapah Basin.

*Eastern Ghats Belt*

The Eastern Ghats Belt, a metamorphosed and highly deformed orogenic belt, lies along the eastern margin of the Cuddapah Basin (Fig. 1). The Eastern Ghats Belt experienced multiple tectonothermal events from 1200 – 500 Ma (Upadhyay *et al.* 2009). At 1000 Ma the Eastern Ghats Belt was involved in orogenic events associated with the assembly of the supercontinent Rodinia (Mezger & Cosca 1999) (Upadhyay *et al.* 2009). The youngest tectonothermal event the Eastern Ghats Belt was involved in was the Pan-African orogenesis (530 Ma) (Mezger & Cosca 1999), (Upadhyay *et al.* 2009) related to the formation of Gondwana. The Ongole Domain is a unit of the Eastern Ghats Belt near the eastern margin of the Cuddapah Basin (Fig. 1). It is believed to have a geological history distinct from the rest of the Eastern Ghats Belt (Upadhyay *et al.* 2009). The Ongole Domain, consisting of a high-grade

metasedimentary package, was intruded by felsic plutonic rocks at ~1720 Ma. It then experienced an ultra-high temperature metamorphic and deformation event at 1630 – 1610 Ma which caused reequilibration of the U-Pb isotope system in most zircons in the terrain (Upadhyay *et al.* 2009). At 1450 -1350 Ma the Ongole Domain terrain experienced ductile brittle deformation associated with Mesoproterozoic rifting along the margin of Proto-India (Upadhyay *et al.* 2009). This was followed by a moderate thermal overprint during the early Neoproterozoic (1100 Ma) (Upadhyay *et al.* 2009). A period of felsic magmatism in the Vinjamuru Domain (Fig. 1), near the Ongole Domain gave magmatic zircon ages of $1868\pm6$ and $1771\pm8$ Ma (Dobmeier & Raith 2003). Detrital ages of the Eastern Ghats Belt of ~2500 Ma suggest a possible Dharwar Craton provenance of the original sedimentary package (Upadhyay *et al.* 2009).

*Cuddapah Basin*

The deposition ages of the sediments in the Cuddapah Basin are not very well constrained. Zachariah (1999) used $^{206}Pb$-$^{204}Pb$ systematics to date U-mineralized carbonate horizons of the Vempalle and Tadpatri Formations. A $^{206}Pb$-$^{204}Pb$ age of $1779\pm85$ Ma was obtained for a U-mineralized sample from the Tadpatri Formation and $1752\pm41$ Ma from the Vempalle Formation, interpreted as minimum ages for carbonate sedimentation and dolomitization within the Cuddapah Supergroup. A Rb–Sr whole rock mineral age of $1817\pm24$ Ma for a sill from the Pulivendla was reported by Baskar Rao *et al.* (1995). Anand (2003) found $^{40}Ar$-$^{39}Ar$ laser-fusion ages for the Tadpatri mafic sills to be $1899\pm20$ Ma. French (2008) obtained U-Pb dates of $1885.4\pm3.1$ Ma from baddeleyite for a mafic sill from the Tadpatri Formation. Dating of these sills gives a minimum depositional age for the sediments intruded by the sills.

# Age and Basin Evolution of the Cuddapah Supergroup

A period of potassic magmatism produced kimberlite dykes which intruded the Dharwar Craton and the Nallamalai Group of the Cuddapah Basin (Chalapathi Rao *et al.* 1996). The kimberlites that intruded the lower section of the Nallamalai Group, the Bairenkonda Formation, have been dated using whole rock Rb-Sr methods by Crawford and Compston (1973) giving an age of 1200 Ma and by Rao (1996) using K-Ar dating to give an age of 1350±52 Ma.

The formation and evolution of the Cuddapah Basin is not well understood. It is often interpreted as being a foreland basin to the Eastern Ghats orogen (Dasgupta & Biswas 2006); (Manikyamba *et al.* 2008) largely due to its position next to the Eastern Ghats. However, Singh and Mishra (2002) proposed a different model for the formation of the basins. Gravity profiles across the basin show a broad gravity high and high seismic velocity at shallow depth over the Eastern Ghats and a gravity low towards the eastern side of the Cuddapah Basin and gravity high towards the south western side (Singh and Mishra, 2002). According to these authors, the margin at the time was a suture zone formed by the collision between two continents. Considering this would have occurred in the early Proterozoic it may have been associated with the amalgamation of the supercontinent Columbia. Using this theory they suggest the Cuddapah Basin may have formed as a peripheral foreland basin evolved through Proterozoic continent-continent collision. They also attribute the crescent shape and curvilinear contact zone to continental collision. Another line of evidence for this model would be that the sedimentary sequences are compatible with a shelf to marine origin.

Chaudhuri *et al.* (2002) developed an alternative model where the Cuddapah Basin and other intracratonic basins in India developed in a rift setting. This is based on the existence of deep faults within the Cuddapah Basin exposed by gravity data (NGRI, 1975). They suggest the initial rifts may have followed pre-existing lineaments defined by either Archaean greenstone belts or belts of crustal convergence. Similarly, Hou *et al.* (2008) proposed that the Cuddapah Basin was a rift-type basin formed during the breakup of the Proterozoic Columbia supercontinent.

Gravity modelling based on the results of a deep seismic sounding survey (Kaila *et al.* 1979) across the Eastern Ghats, Cuddapah Basin and Dharwar Craton was carried out by Kaila and Bhatia (1981). The results show a steep positive gradient anomaly observed in the eastern margin of the Cuddapah Basin, which corresponds at the surface to the thrust contact with the Eastern Ghats. Kaila and Bhatia (1981) attributed this anomaly to the presence of a high density mass at shallow depth along the low-angle fault in the region. This high-density material could be deep mantle rocks brought up along the thrust at the eastern margin of the Cuddapah Basin. Further evidence of deep-seated faults are reported throughout the Cuddapah Basin (Kaila and Bhatia, 1981), supporting theories of a rift-setting or suggesting the possibility that this was a fault controlled basin.

## Methods

*Sequence Stratigraphy*

Three stratigraphic sections were logged in the Cuddapah Basin (Fig. 13-15). These covered the (1) Gulcheru Formation and base of the Vempalle Formation, (2) the

Pulivendla and Tadpatri Formations and (3) the Bairenkonda Formation and the base of the Cumbum Formation. A pseudo-gamma ray log, as well as a log of uranium, thorium and potassium content for the sediments was measured for each section, using a portable Gamma Ray Spectrometer. These stratigraphic and geophysic logs are used for assisting in the interpretation of the depositional environment and basin evolution of the Cuddapah Basin.

*Cross Section*

Structural data was collected along a section east-west across the basin (Fig. 4). These data, along with map data imported from a georeferenced geological map of the Cuddapah Basin (Meijerink *et al.* 1984), were used to create an unbalanced cross-section of the basin.

*U-Pb zircon geochronology*

Samples were selected from the Papaghni, the Chitravati and Nallamalai Groups for U-Pb zircon geochronological analysis to constrain maximum depositional ages and changes in provenance up the sequence. Whole rock samples were crushed using a jaw crusher then milled using a tungsten carbide mill and sieved through a 425µm mesh and a 75µm mesh. Sample that was between 425 and 75µm was washed with water and detergent to remove dust and hand panned to separate heavy minerals. This concentrate was then passed through methylene iodide heavy liquid separation to isolate minerals with a density greater than 3.3 g cm$^{-3}$. The heavy mineral separate was then washed with acetone, dried and passed over with a neodymium magnet to remove heavy magnetic minerals. After this step, sample CU10-21 was found to have

no grains that were identified as zircons in the separate, some crushed but unpanned sample was then sent to Minsep Laboratories in Denmark, WA, to be separated. Zircons were then hand picked from the other three samples and mounted in epoxy resin. Mounts were then polished and carbon coated for imaging using a Philips XL20 scanning electron microscope. Images were obtained using backscattered electron and cathodoluminescence to view zonation in individual grains.

Laser Ablation – Inductively Coupled Plasma Mass Spectrometry (LA-ICMPS) U-Pb analysis was carried out using an Agilent 7500cs ICPMS coupled with a New Wave 213 nm Nd-YAG laser at Adelaide Microscopy. Zircons were ablated in a helium atmosphere, using a beam diameter of 30 μm, frequency of 5 Hz and a laser intensity of 75%. Data acquisition involved 40 seconds of background measurement, 10 seconds of beam stabilisation, and 50 seconds of sample ablation. Ablation and machine fractionation was corrected using the GEMOC GJ-1 standard (normalisation data: $^{207}Pb/^{206}Pb$ = 608.3 Ma, $^{206}Pb/^{238}U$ = 600.7 Ma and $^{207}Pb/^{235}U$ = 602.2 Ma) (Jackson $et\ al.$ 2004) and was further monitored using an internal standard Plesovice (337.13 ± 0.37 Ma, (Slama $et\ al.$ 2008)). GJ-1 gave a mean age of 600.5±1.6 Ma and MSWD 0.36 and Plesovice gave a mean age of 331.7±2.7 and MSWD 3.3. These results are within error of the TIMS ages known for the standards, ages calculated are therefore valid. Age calculations were conducted using GLITTER software (Van Achterbergh $et\ al.$ 2001). Concordia diagrams and probability distribution curves where constructed using the Isoplot macro (version 4.11) (Ludwig 2003). For zircons older than 1 Ga the $^{206}Pb/^{207}Pb$ age was used. For zircons younger than 1 Ga the $^{206}Pb/^{238}U$ age was used.

*Hf Isotope Analysis*

In-situ Hf isotope data were collected with a Thermo-Scientific Neptune Multi Collector ICP-MS coupled to a New Wave UP-193 Excimer laser (193nm) at Waite Campus, University of Adelaide, following procedures of Payne et al. (in prep). The samples analysed were two of the four used for LA-ICPMS analysis. Concordant zircon grains (90-110% concordance) were analysed in the same CL domain as they were for U-Pb LA-ICPMS geochronology. The laser conditions were 4ns pulse length, 5 Hz with a 50 um spot size (~10J/cm$^2$). The ablated material travelled through a He ablation atmosphere mixed with Ar sample gas. Set-up of the system prior to ablation sessions was conducted using analysis of JMC475 Hf solution and an AMES Hf solution. $^{171}$Yb, $^{173}$Yb, $^{175}$Lu, $^{176}$Hf, $^{177}$Hf, $^{178}$Hf, $^{179}$Hf and $^{180}$Hf were measured on Faraday detectors with $10^{12}\Omega$ amplifiers and an integration interval of 0.232 seconds. Hf mass bias was corrected using exponential law fractionation correction using a stable Hf isotope ratio of $^{179}$Hf/$^{177}$Hf=0.7325. Yb isobaric interference on $^{176}$Hf was corrected by direct measurement of Yb fractionation using $^{171}$Yb/$^{173}$Yb coupled with the Yb isotopic values of (Segal *et al.* 2003). The applicability of these values were verified by analysing JMC 475 Hf solutions doped with varying levels of Yb with interferences up to $^{176}$Yb/$^{177}$Hf= ~0.5. Lu isobaric interference on $^{176}$Hf was corrected using a $^{176}$Lu/$^{175}$Lu ratio of 0.02655 (Vervoort *et al.* 2004) assuming the same mass bias behaviour as Yb. For Yb signals below 10 mV, interference corrections were made using an empirically derived $^{176}$Yb/$^{173}$Yb ratio and the Hf mass bias factor similar to the method described by (Griffin *et al.* 2000). This was done as the potential errors involved in the method are outweighed by the significantly greater uncertainty caused by the small Yb beam. In this case an empirically derived ratio of 0.739689 was used. This was derived by analysis of a

series of Yb and Hf doped glass beads. Confirmation of accuracy of the technique for zircon analysis was monitored using a combination of the Plesovice (Slama *et al.* 2008), Mudtank and QGNG standards.

*Stable Isotopes*

Carbonate samples were cut to expose a clean surface, which was then drilled to produce a fine powder. δ13C and δ18O isotope data were acquired simultaneously on a Micromass Isoprime dual inlet mass spectrometer at L'Université du Québec à Montréal. Approximately 100 μg of powder was reacted in singular glass reaction cells with purified $H^3PO^4$ at 90ºC for 10 minutes while being constantly cryogenically trapped. Evolved $CO^2$ was cryogenically distilled then measured against an in-house reference gas. δ18O was corrected for equilibrium with H2O during reaction using the Craig (1957) equation and both δ13C and δ18O samples were calibrated to VPDB using an in-house calcite standard. All δ13C and δ18O are reported with respect to the Vienna Pee Dee Belemnite (VPDB) as per mil deviations.

# Sedimentary Observations

*Gulcheru Formation*

The Gulcheru Formation is the basal formation of the Cuddapah Supergroup, unconformably overlying the Archaean Dharwar Craton, which forms the basement of the Cuddapah Basin. The stratigraphic log of the Gulcheru Formation (Fig. 13) was made at GPS location 15º46'6.9"N, 78º3'23.4"E (Fig. 1), near the village of

Tandrapadu. The Gulcheru Formation displays different thicknesses and facies changes laterally but generally shows a fining up followed by a coarsening up. The basal facies is characterised by alternating 0.5-2 m beds of conglomerates with 1-10cm angular quartz grains in a fine grained clay matrix and beds of unsorted sandstone with 1-3 mm quartz grains and medium grained sand matrix (Fig. 6a). Clasts are predominately of vein quartz with some dark layers rich in mafic minerals. This facies displays channels with depths up to 10cm, planar cross bedding (Fig. 6b) and trough cross bedding (Fig. 6c) and laminations from elevation 3 to 17 m on the stratigraphic log (Fig. 13). Sediments gradually fine up, starting at elevation 17 m on the stratigraphic log (Fig. 13) and consist mostly of coarse grained sandstone with sub-rounded white quartz grains with some finer grained sandstone beds developing. Cross-bedding at the base of the formation gives palaeocurrent towards 65º and 129º (Fig. 13). Trough bedding and ripples give directions 237º to 320º (Fig. 13) through the rest of the sequence. Cross bedding and channels are common throughout the sequence and mudcracks occur in the upper section of the formation. Conglomerate beds mark the upper contact of the Gulcheru Formation with a sudden transition to shales, characteristic of the Vempalle Formation. In another location to the south, GPS location 15º32'47.8"N, 78º2'21.8"E, the lower contact (Fig. 6d) was seen again and varied very slightly. Here, shale beds started developing 3 m from the base of the formation and channels were filled with shales or very coarse grained conglomerates (Fig. 6e). Conglomerate layers contained sub-angular quartz clasts up to 5 cm (Fig. 6f).

*Vempalle Formation*

The stratigraphic log of the base of the Vempalle Formation (Fig. 13) was made at GPS location 15º46'6.9"N, 78º3'23.4"E (Fig. 1), near the village of Tandrapadu. This formation was also seen near the village of Gattimanikonda, GPS location 15º31'8.9"N, 78º10'34.6"E and further south; 15º30'38.4"N, 78º10'17.5"E and in a mine near Kolumalapalle, GPS location 15º28'31.9"N, 78º7'58.5"E.  The upper part of the Gulcheru Formation displays very coarse sandstone. A sharp transition occurs then to a thick lithified package consisting mostly of shales with some minor interbedded fine-grained sandstone with symmetric ripples at the base of the formation and mudcracks (Fig. 7a) on fine sand beds 6 m from the base of the formation.  This facies corresponds to the basal part of the Vempalle Formation. Gamma ray spectrometry data correlates well the lithology at this transition point between the Gulcheru Formation and the Vempalle Formation; an increase in potassium, uranium and total gamma count at elevation 38 m on the stratigraphic log (Fig. 13) represents a sudden transition to shales from coarse grained sandstones. The formation then develops into interbedded dolomites, dolomitic limestones and shales (Fig. 7b).  The transition between the shale rich basal facies and these carbonate rich facies that are characteristic for the rest of the formation was not observed. Laminated stromatolitic dolomite beds (Fig. 7c) occur interbedded with grainstone (Fig. 7d) made up of broken stromatolite, ooids (layered spherical calcium carbonate sedimentary grains) and oncoids (layered spherical structures formed by cyanobacterial growth, similar to stromatolites) that fill the gaps between stromatolites and thin (0.5-10 cm) layers of chert that often cap (Fig. 7e) stromatolite beds.  Purple-pink shales beds are also found interbedded throughout the stromatolitic dolomites (Fig. 7f).

*Pulivendla Formation*

The upper 20 m of the Pulivendla Formation was located at GPS location 15º21'3.5"N, 78º85'10.5"E (Fig. 1), 44 km WSW from Nandyal, this is the location of the stratigraphic log (Fig. 14) of this sequence of the Pulivendla Formation. The contact between the Vempalle Formation and the Pulivendla Formation was not observed. Some authors (Meijerink *et al.* 1984, Riding & Sharma 1998, Dasgupta *et al.* 2005) have reported an unconformity at this contact. The Pulivendla Formation consists of medium grained sandstones with pale sub-rounded well sorted quartz grains. These sandstones display dark laminations, cross bedding (Fig. 8a), mud cracks (Fig. 8b), reactivation surfaces, parting lineations and symmetrical ripples (Fig. 8c). Symmetrical ripples had a crest lineation dipping in the direction 268º suggesting a bidirectional palaeocurrent of 178º/358º. Near the top, contact sandstones become finer grained with more angular, less sorted grains and develop shale beds which mark the gradual transition into the Tadpatri Formation (elevation 12-22 m on the stratigraphic log, Fig. 13); this corresponds to an increase in potassium, uranium, thorium and total gamma count in the stratigraphic log (Fig. 14) as would be expected when changing from sands to shales.

*Tadpatri Formation*

The stratigraphic log (Fig. 14) of the Tadpatri Formation was located at GPS location 15º21'3.5"N, 78º85'10.5"E (Fig. 1), 44 km WSW from Nandyal. This formation was also seen in a mine near Yagantipalle, GPS location 15º18'59.7"N, 78º11'40.8"E, near Komarolu (15º33'39.4"N, 78º10'17.9"E) and near Sugali Mitta (15º33'41.9"N,

78º70'22.7"E). The lower contact of the Tadpatri Formation is a gradual change from fine grained sandstones of the Pulivendla Formation to interbedded shale and sandstone beds that develop into continuous shale beds seen at elevation 22-48 m on the stratigraphic log (Fig. 14). Fine grained sand beds develop; seen at elevation 48-53 m on the stratigraphic log (Fig. 14) fining up into a 10 m sequence of laminated silts and 50-100 cm silicified carbonate beds with stromatolites (Fig. 9a) and channels. The carbonate beds correspond with a drop in potassium, uranium, thorium and total gamma count to below detection level at elevation level 62 m on the stratigraphic log (Fig. 14). At a mine near Yagantipalle (15º18'59.7"N, 78º11'40.8"E) volcanics and intrusive igneous rocks were observed in the Tadpatri Formation. A highly weathered 40m thick intermediate sill (Fig. 9b) with $CO_2$ alteration intrudes over a black carbon rich shale layer (Fig. 9c). Above the sill are shale and dolomite beds. At an outcrop near Komarolu (15º33'39.4"N, 78º10'17.9"E) a bed of dark mafic volcanic rock of unknown thickness was found in contact with a sequence of grey laminated dolomite (Fig. 9d) with thin chert layers and beach rosettes (shallow water sedimentary features that indicate lightly breaking wave movement in an upper tidal environment) (Fig. 9e). The top contact of the Tadpatri Formation is an unconformity; the only area where this was observed was at 15º21'3.5"N, 78º85'10.5"E, 44 km WSW from Nandyal. In this area the top of the Tadpatri Formation was an angular unconformity (Fig. 9f) overlain with sandstones of the Banaganpalle Formation of the younger Kurnool Group.

*Gandikota Formation*

The Gandikota Formation was observed near Itikyala, GPS location 15º3'21"N, 78º5'48.4"E. The Gandikota Formation is a well bedded medium grained mature

sandstone (Fig. 10a) with rounded quartz grains and 2-3 cm sandstone concretions (Fig. 10b) that have weathered away in areas and conjugate quartz veins (Fig. 10c). It displays trough bedding in two directions, 180º from each other, ripples, cross bedding (Fig.10d) and evidence of dune movement. Symmetric ripples show a bidirectional palaeocurrent of 070º/250º.

*Bairenkonda Formation*

The stratigraphic log of the Bairenkonda Formation (Fig. 15) was located primarily at Gandleru River, near Gajulapalli (15º23'34.2"N, 78º39'48.4"E). The formation was also observed at 15 locations along Giddalur Road between Gandleru River, near Gajulapalli (15º23'34.2"N, 78º39'48.4"E) and Nandikanama Pass (15º25'24.3"N, 78º45'42.2"E) when data for a cross section was collected. The lowest sequence of the Bairenkonda Formation that was observed (>9 m thick) is composed predominantly of quartz rich medium grained laminated sandstones (Fig. 15). A bed of dark fine grained mafic volcanogenic sediments (elevation 4-7 m on the middle section of the stratigraphic log, Figure 15) lies over the laminated sandstone and contains large rafts of quartz rich medium grained laminated sandstone, very similar to the underlying sandstone, suggesting the volcanic layer flowed over semi-consolidated sediments below. Directly above the volcanic layer is a 10 m sequence of sandstones; the basal facies of this sequence is a fine grained sandstone (Fig.11a) with small ripples and parting lineations. The parting lineations and symmetric ripples give bi-directional palaeocurrent directions 12º/192º and 90º/270º (Fig. 15). This facies gradually develops into a pale homogenous coarse grained 30-40 cm sandstone bed (Fig.11b) with crossbedding and localised concentrations of medium grained red chert clasts, then makes a sharp transition to a heavy mineral laminated

medium grained sandstone followed by a very thin layer of clay, mostly eroded away. This pattern is then repeated twice at elevation 8 -15 m on the middle section of the stratigraphic log (Fig. 15). The top of the formation elevation 0-3 m on the top section of the stratigraphic log (Fig. 15) is a pale massive sandstone with beds up to 2 m thick, very quartz rich (Fig. 11c) except for thin layers with high concentrations of well rounded red chert clasts. This sandstone also contains some 10-20 cm tuffaceous layers. This facies shows bar migration (Fig. 11d) and adhesion ripples, sedimentary structures formed by wind blowing dry sand over moist sand (Fig. 11e). The transition into the Cumbum Formation is marked by an appearance of shale beds and an increase in uranium, potassium, thorium and total gamma count at elevation 1.5-3 m on the top section of the stratigraphic log (Fig. 15). Near the top contact of the formation symmetric ripples (Fig. 11f) give consistent bi-directional palaeocurrents of 75°/255°.

*Cumbum Formation*

The Cumbum Formation was observed at Nandikanama Pass (15º25'24.3"N, 78º45'42.2"E), at the contact between the Bairenkonda Formation and the Cumbum Formation. This is where the stratigraphic log (Fig. 15) showing the base of the Cumbum was recorded. The basal contact of the Cumbum Formation is a gradual change from sandstones (Fig. 12a) to shale beds (Fig. 12b) showing a transitional change from the Bairenkonda Formation to the Cumbum Formation. Uranium, potassium, thorium and total gamma count all increase significantly at the transition to the Cumbum Formation. The basal shales and sandstones then develop into finely laminated, very fine grained sandstone or shales with small ripples. Overlying these

are dark grey shales with ~1 cm bedding (Fig. 12c) and layers that are rich in tabular limestone clasts (Fig. 12d).

# Stratigraphic evolution and model of deposition

*Gulcheru Formation*

Coarse sand beds featuring asymmetrical ripples, mudcracks and channels suggest a fluvial system or shallow marine environment. The presence of ripples indicates the presence of running water at the time of deposition; asymmetrical ripples indicate a current running in one direction; for example a river or stream. Ripples can also give a palaeocurrent, the direction the current was running at the time of deposition. Mudcracks suggest the presence and then removal of water; they are formed by moist muds or sands drying, causing cracking and being covered by more sediment before they are destroyed. The grain shape and sorting of the conglomerate beds suggests the sediments did not travel far before deposition. The asymmetrical ripples suggest a current moving in one direction. Current was measured to be towards the east at the base of the formation (Fig. 13). Sedimentary features and grain shape and size suggest the base of the formation was deposited in an alluvial fan setting with high energy sheet flows. Sediments fine up throughout the formation; this could be due to lateral movement of the alluvial fan and these sediments could represent the outer limits of the fan, or the depositional environment could be changing to a fluvial setting. Asymmetrical ripples and cross bedding higher in the Gulcheru Formation show palaeocurrent direction towards the west (Fig. 13). The top of this formation shows a sharp flooding surface with an abrupt change in energy from a conglomerate

bed to a thick sequence of shales corresponding to an increase in uranium, potassium and total gamma count at elevation 38 m on the stratigraphic log (Fig. 15); suggesting a transition to deep a marine environment or a loss of sediment supply. The Gulcheru Formation is interpreted to represent an alluvial fan to fluvial depositional setting.

*Vempalle Formation*

Sequences of stromatolitic limestones and dolomites alternating with grainstone beds made up of grains of stromatolite, ooids and oncoids and chert layers suggest strong storms causing break up of stromatolites and deposition of grainstone beds, where cherts are interpreted as erosional surfaces indicating periods of exposure. This is interpreted as a supertidal environment. Shale beds generally indicate low energy depositional environments; within this sequence they could indicate transitions to lagoonal depositional environments or a slightly deeper environment with a loss of sediment source. The Vempalle Formation is interpreted to have been deposited in a shallow marine or lagoonal setting. This formation represents a period of either relative sea level rise or a loss of sediment source.

*Pulivendla Formation*

The Pulivendla Formation consists of medium to coarse grained sands, cross-bedding, reactivation surfaces, symmetrical ripples and parting lineations within the Pulivendla Formation. Parting lineations are sedimentary structures in which sand grains are aligned in parallel lines on the surface of a sand layer, they can be used to determine the depositional environment as they indicate the presence of running water and can be used to find palaeocurrent direction. Symmetrical ripples are formed by a current

moving in two opposite directions; for example, wave movement. Symmetrical ripples showed a bi-directional palaeocurrent trending north-south (Fig. 14). The Pulivendla Formation was deposited in a high energy shallow subtidal environment.

*Tadpatri Formation*

The base of the Tadpatri Formation displays a transition from sands to a 30 m thick sequence (Fig. 14) of shales. This is interpreted to represent a rise in sea level to a low energy deep subtidal environment or indicate a loss of sediment source. Higher up in the Tadpatri Formation at elevation 55 m and 63 m on the stratigraphic log (Fig. 14) beds of carbonate rich sediment are abundant in stromatolites. The stromatolitic carbonates suggest a shallow subtidal environment with little or no sediment supply. Beach rosettes, observed in shales interbedded with dolomitic beds observed within the Tadpatri Formation, indicate an intertidal to foreshore environment, with beach rosettes suggesting breaking waves. The Tadpatri Formation represents a low energy shallow marine environment.

*Gandikota Formation*

The Gandikota Formation consists of medium grained, mature quartzite with asymmetrical ripples and evidence of dunes. Asymmetrical ripples indicate the presence of water with a unidirectional current. Palaeocurrent direction was from the west to east. Dunes suggest aeolian influences, possibly a shoreline environment. The Gandikota Formation was deposited in a fluvial to shoreline environment with a lot of sediment that travelled far from its source.

*Bairenkonda Formation*

The Bairenkonda Formation generally consists of medium to coarse grained sandstones. Parting lineations, bar migration and symmetrical ripples are evident throughout the Formation and all suggest the presence of water. Palaeocurrent indicators, ripples and parting lineations, give a range of bidirectional currents. Both north-south to west-east directions were measured. These features indicate an intertidal environment. Laminations and thin layers of clay observed in some of the facies suggest cycles of high and low energy, particularly at elevation 8 -15 m on the middle section of the stratigraphic log (Fig. 15), although the clay layers may also represent periods of loss of sediment source. The sediments of the Bairenkonda Formation represent shoreface, shallow to emergent environments. There is evidence of volcanism during the deposition of the Bairenkonda Formation, mafic volcanogenic beds were observed within the formation (elevation 4-7 m on the middle section of the stratigraphic log, Figure 15).

*Cumbum Formation*

The base of the Cumbum Formation showed a short transitional sequence from sandstones to shales. A change to shales suggests a low energy environment. Large (2-10 cm) pieces of dolomite (Fig. 12) within shales suggest strong storms breaking up limestone and rapid transportation to deep water. Uranium, thorium, potassium and total gamma count values increase at the transition to the Cumbum Formation. The high values of radioactive elements may reflect the change to more shale rich facies or could suggest a different source of sediments or a high influx of sediments adding more radioactive minerals to the basin. The Cumbum Formation is interpreted to represent a rise in sea level, with the environment gradually getting deeper.

## Cross Section

Two cross sections of the same transect were created, with different interpretations of what occurs at depth. The western side of both cross sections displays simple shallow east dipping beds.  The Kurnool Group overlie Cuddapah Supergroup sediments with an unconformable relationship.   Kurnool Group sediments are not deformed suggesting they were deposited after Nallamalai Group sediments were deformed.  At least one fault related fold is evident at the eastern margin of the basin.  This fault originates in the Tadpatri Formation.  It has been interpreted this way due to the high levels of shales in the Tadpatri Formation.  This fold is asymmetrical with shallow dipping limbs on the east side suggesting thrusting is coming from that direction. This indicates the deformation of the Eastern Ghats as the source of the main stress. Folds slightly to the west of these folds are detachment folds showing less shortening than the fold to the east; this supports the theory that the main stress is coming from the east.

The deep thrust fault that is shown in the first cross section is indicated by Meijerink *et al.* (1984)'s map and is included because very little is known about the contact between the Nallamalai Group sediments and the Kurnool Group, as this contact was not observed.  This cross section suggests the Nallamalai Group sediments were deposited after this faulting event and it is unclear what the relationship between the Nallamalai Group sediments and the Kurnool Group sediments is.  The second cross section shows all the formations continuing along the basin and indicates a

depositional history in which the Nallamalai Group sediments were deposited onto the older Cuddapah Supergroup sediments. These were deformed, some sediments were eroded away and then the Kurnool Group was deposited.

# U-Pb zircon geochronology results

*CU10-01*

This sample was taken 20 metres up from the base of the Gulcheru Formation which corresponds to the base of the stratigraphic succession in the Cuddapah Basin (Fig. 2) at GPS location 15º46'6.9"N, 78º3'23.4"E (Fig. 1), near the village of Tandrapadu. The sample was taken from a microconglomerate with 0.2 – 1.5 cm size sub-angular quartz grains and a fine grained matrix with centimetre scale planar and cross bedding. This microconglomerate was part of a 15 m sequence that graded from a coarse conglomerate with cobble sized grains through the sampled microconglomerate and into bedded sandstone. Fifty analyses were obtained from 48 zircon grains. U-Pb analyses yielded $^{207}Pb/^{206}Pb$ ages that ranged from 2198±18 - 2599±18 Ma. The eight 90-110% concordant analyses yielded $^{207}Pb/^{206}Pb$ ages that ranged from 2502±17 - 2588±17 Ma with major peaks in probability density distribution plots at 2532±20 Ma and 2583±21 Ma. The youngest 90-110% concordant analysis (spot cu10_01_15) yielded a $^{207}Pb/^{206}Pb$ age of 2502±17 Ma (91% concordant) (Fig. 16).

*CU10-19*

This sample was taken from the Pulivendla Formation near the transitional contact with the Tadpatri Formation (Fig. 2) at GPS location 15º21'3.5"N 78º85'10.5"E (Fig. 1), 44 km WSW from Nandyal. The sample was taken from a coarse grained sandstone with 1 – 15cm beds and sub-angular lithic clasts. This sandstone was the base of a sequence that graded gradually into shale beds. Fifty analyses were conducted from 48 zircon grains. Eight of these were 90-110% concordant. U-Pb analyses yielded $^{207}Pb/^{206}Pb$ ages that ranged from 1112±22 - 3070±15 Ma. The eight 90-110% concordant analyses yielded $^{207}Pb/^{206}Pb$ ages that ranged from 1899±19 - 2552±17 Ma with major peaks in probability density distribution plots at 1931±17 Ma and 2514±83 Ma. The youngest 90-110% concordant analysis (spot CU1019_41) yielded a $^{207}Pb/^{206}Pb$ age of 1899±19 Ma (100% concordant) (Fig. 17).

*CU10-10*

This sample was taken from the Bairenkonda Formation, which is stratigraphically below the Cumbum Formation; these two formations make up the Nallamalai Group; the highest group in the Cuddapah Supergroup sequence (Fig. 2). The sample was taken from GPS location 15º23"34.2"N 78º39"40.4"E (Fig. 1) near the town of Gadzulapalle. This coarse grained sandstone was part of a 6 m sequence of 30 - 40 cm sand beds with thin millimetre-scale clay beds between sand beds. Fifty analyses were obtained from 49 zircon grains. Fourteen of these were 90-110% concordant. U-Pb analyses yielded $^{207}Pb/^{206}Pb$ ages that ranged from 1580±24 - 3459±17 Ma. The fourteen 90-110% concordant analyses yielded $^{207}Pb/^{206}Pb$ ages that ranged from 1659±22 - 3007±16 Ma with major peaks in probability density distribution plots at

1805±25 Ma and 2514±20 Ma. The youngest 90-110% concordant analysis (spot cu10_10_40) yielded a $^{207}$Pb/$^{206}$Pb age of 1660±22 Ma (96% concordant) (Fig. 18).

*CU10-21*

This sample was taken from the Cumbum Formation, the stratigraphically highest formation in the Cuddapah Supergroup (Fig. 2) at GPS location 15º25'21.9"N 78º45'18.4"E (Fig. 1). The sample was taken from a fine to medium grained sandstone with stylolites. The sandstone was part of a 2 m sequence of alternating sand and shale 10 – 40 cm beds. This was near the transitional contact between the Bairenkonda Formation and the Cumbum Formation. Twenty analyses from 20 zircon grains were conducted. Seven of these were 90-110% concordant. U-Pb analyses yielded $^{206}$Pb/$^{238}$U ages that ranged from 326±5 - 2561±29 Ma and $^{206}$Pb/$^{207}$Pb ages that ranged from 512±32 - 3400±26 Ma. The seven 90-110% concordant analyses yielded $^{206}$Pb/$^{238}$U ages that ranged from 913±11 - 2790.2±17 Ma and $^{206}$Pb/$^{207}$Pb ages that ranged from 919±24 - 2790±17 Ma with a major peak in probability density distribution plots at 1753±60 Ma. The youngest 90-110% concordant analysis (spot cu1021_01) yielded a $^{206}$Pb/$^{238}$U age of 913±11 Ma (99% concordant) (Fig. 19).

# Hf Isotope Results

Results from the Hf isotope analysis (Table 3) plot above the depleted mantle line (Fig. 5), this indicates that there is something wrong with the data (Payne, *pers. comm.*), to try to identify the problem the $^{176}$Hf/$^{177}$Hf and $^{176}$Yb/$^{177}$Hf ratios within

four single zircon analyses were plotted against each other (see Fig. 5) and some of these showed a positive correlation of $^{176}Hf/^{177}Hf$ and $^{176}Yb/^{177}Hf$. Positive correlation between these two ratios is generally considered to be an analytical error as this is unlikely to occur naturally, although there are some possible scenarios where this could occur naturally, such as if the depleted mantle is unusually enriched in rare earth elements and depleted in Hf. However this is unlikely and would not explain both problems with the data so the data will not be used in this study. This error may have been caused by direct rare earth element interference from $^{176}Lu$ and $^{176}Yb$. However this should not have been an issue as standards and initial set up suggest this error was being over corrected (Payne, *pers. comm.*). Alternatively it may have been caused by rare earth oxide interference caused when $^{160}Gd$ and $^{160}Dy$ combine with $^{16}O$.

## Stable Isotopes Results

Three samples were analysed to collect δ13C and δ18O isotope data (Table 4). Two samples; T1 and T2, taken from the Tadpatri Formation were analysed. These samples were from stromatolitic dolomites 1.5 m stratigraphically apart (15º33'39.4"N, 78º10'17.9"E). One sample; V1, from the Vempalle Formation was from a stromatolitic dolomite (15º30'38.4"N, 18º10'17.5"E). The δ13C values of these samples range between -1.54 and +1.45 ‰. Comparison of isotopic values with published data indicates that moderately positive δ13C values (up to +4.0‰) are characteristic of the interval between 1250 and 800 Ma (Bartley *et al.* 2001). This pattern is distinct from that of younger Neoproterozoic successions, which typically

record values >+5‰, and older Mesoproterozoic successions, which record values near 0±1‰, and suggests that these moderately positive values may be useful for broad time correlation (Kah *et al.* 1999, Bartley *et al.* 2001). The δ13C values of these samples can be correlated with known early Mesoproterozoic (before 1300 Ma) δ13C values. Sample V1 with a δ13C value of 1.45‰ could have been formed at the times between 1250 and 800 Ma when δ13C values dropped, however this would not correlate with that age data for the Vempalle Formation, which is the oldest formation in the Cuddapah Basin containing carbonates. Ideally more stable isotope data is needed for the carbonates deposited in the Cuddapah Supergroup to be able to correlate them with more confidence.

# Discussion

*Age Constraints on Deposition of the Cuddapah Supergroup*

The only direct age constraints previously published have provided minimum depositional ages for single formations within the Cuddapah Supergroup (1752 Ma (Zachariah *et al.* 1999) for the Vempalle Formation, 1817 Ma (Baskar Rao *et al.* 1995) for the Pulivendla Formation, 1779 Ma (Zachariah *et al.* 1999), 1899 Ma (Anand *et al.* 2003) and 1885 Ma (French *et al.* 2008) for the Tadpatri Formation and 1200 Ma (Crawford and Compston 1973) and 1350±52 Ma (Rao *et al.* 1996) for the Bairenkonda Formation).

This study provided new maximum depositional ages on the different sedimentary packages within the Cuddapah Supergroup. All zircons are interpreted as being detrital zircons as all samples were taken from sandstones that have undergone no tectonothermal event that would create or alter zircons. The age given by the youngest 90-110% concordant analysis is interpreted as the maximum depositional age for the formation.

U-Pb zircon geochronology on four sandstones from four formations (Gulcheru Formation, Pulivendla Formation, Bairenkonda Formation, and Cumbum Formation) throughout the Cuddapah Supergroup constrains the maximum depositional age of each of these formations and of the Cuddapah Basin. The maximum depositional age of the Gulcheru Formation, is 2502±17 Ma. The Gulcheru Formation corresponds to the base of the stratigraphic succession in the Cuddapah Basin, thus this age marks the onset of sedimentation and maximum age for the formation of the basin. Maximum depositional ages obtained in this study are 1899±19 Ma for the Pulivendla Formation, 1660±22 Ma for the Bairenkonda Formation and 913±11 Ma is interpreted as being the maximum depositional age for the Cumbum Formation. This Cumbum Formation is the youngest formation dated in this study.

My results, together with previous work (Crawford & Compston 1973, Baskar Rao *et al.* 1995, Chalapathi Rao *et al.* 1996, Zachariah *et al.* 1999, Anand *et al.* 2003, French *et al.* 2008), constrain the timing of deposition of the different formations constituting the Cuddapah Supergroup:

- The Gulcheru Formation and Vempalle Formation had been deposited between ~2502 and 1899 Ma.

- The Pulivendla Formation and Tadpatri Formation were deposited between 1919 and 1879 Ma

- The Bairenkonda Formation was deposited after 1660±22 Ma and intruded by kimberlites at 1350±52 Ma, constraining deposition to this time interval

- The Cumbum Formation was deposited after 913±11 Ma.

In total, deposition of the Cuddapah Supergroup extended for ~986 million years.

Stable isotope data from the Tadpatri and Vempalle Formations appear to correspond with known late Palaeoproterozoic to early Mesoproterozoic values. This data is not very conclusive as it was not a robust stable isotope study, however it can be used to support the U-Pb geochronological data.

*Provenance of Sediments*

Samples analysed are from sediments that have undergone no tectonothermal event that would create or alter zircons deposited in the sediments. Laser ablation spots were also taken from cores of zircon grains and any rims identified in CL imaging were avoided. This means all zircon ages reflect tectonothermal events affecting the area the sediments are sourced from. The assignment of source regions based entirely on age correlations with detrital populations is prone to error (Howard *et al.* 2009) - largely due to events of similar ages occurring in multiple locations. However, it is possible to constrain the source of sediments by matching the age of detrital zircons in sediments with the age of potential sources. Detrital peaks from U-Pb geochronology in this study (Fig. 16-19) are here compared to reported ages of rocks of the Dharwar Craton and the Eastern Ghats, in order to speculate on sediment provenance. Detrital zircons analysed vary greatly in morphology, but most are

fragmented and often have rounded edges (Fig. 15-18). This wide range of zircon populations suggests numerous sediment sources draining into the Cuddapah Basin.

Hf isotope data was collected in the hope of constraining potential source regions more accurately; however, due to errors in the Hf isotope results, this data can not be used for this purpose in this study. Future work involving new Hf isotope data on these samples would be very useful in correlation with the U-Pb geochronological results from this study.

Detrital peaks at ages 2600-2500 Ma are evident in probability density distribution plots of samples CU10-01 (2532±20 Ma and 2583±21 Ma), CU10-19 (2514±83 Ma) and CU10-10 (2514±20 Ma) indicating a possible shared source for the Gulcheru Formation, Pulivendla Formation and Bairenkonda Formation. These zircons are potentially sourced from the late Archaean (2600-2500 Ma) granitic intrusions that dominate the eastern part of the Dharwar Craton which form the latest magmatic event in the craton (Jayananda *et al.* 2000). A geochemical analysis by Chakrabarti *et al.* (2009) of the Mesoproterozoic clastic sedimentary rocks of the basal Gulcheru Formation of the Cuddapah Basin point to a mixed felsic-mafic provenance of the Gulcheru rocks occurring as crystalline granites and gneisses and greenstone belts of eastern Dharwar Craton. This supports the geochronological evidence of this study for a Dharwar Craton provenance for the Gulcheru Formation.

There is a peak in the probability density distribution plot at 1931±17 Ma in the sample CU10-19 from the Pulivendla Formation. The zircons making up the 1931±17 Ma peak may be from a 1900 Ma event of large scale mafic/ultramafic

magmatism associated with intracontinental rifting and basin development (French *et al.* 2008). This large igneous province spans the Bastar Craton, the Dharwar Craton and the Cuddapah Basin.

Peaks in density distribution plots at 1805±25 Ma and 1753±60 Ma from samples CU10-10 and CU10-21 respectively could possibly represent the same event as the uncertainties on both ages are reasonably high. A period of felsic magmatism in the Vinjamuru Domain, near the Ongole Domain of the Eastern Ghats has produced ages of 1868±6 and 1771±8 Ma (Dobmeier & Raith 2003) that may have been the source of these peaks, however this event is not very well constrained. The Ongole Domain of the Eastern Ghats (Fig. 1) was intruded at 1720-1700 Ma (Dobmeier & Raith 2003); this may be the source of the 1753±60 Ma peak.

Detrital zircon ages suggest that the Gulcheru Formation and the Pulivendla Formation are both sourced from the Dharwar Craton. At least two sources for the Pulivendla Formation appear to be from within the Dharwar Craton. The Bairenkonda Formation contains zircons that may be sourced from the Dharwar Craton and the Eastern Ghats. The Cumbum Formation appears to be sourced solely from the Eastern Ghats. Further evidence for this is the presence of a 913±11Ma zircon grain, probably associated with the deformation and metamorphism that occurred around 1100-920 Ma due to the Eastern Ghats' involvement with the assembly of the supercontinent Rodinia (Mezger & Cosca 1999, Upadhyay *et al.* 2009). Although there is only a single zircon of this age it does support the theory that these sediments are sourced from the Eastern Ghats. There is also an increase in

radioactive elements (Fig. 15) from the Bairenkonda Formation to the Cumbum Formation which is compatible with erosion from the uplifted Eastern Ghats.

The provenance of the sediments filling the Cuddapah Basin is largely consistent with the Dharwar Craton. Some variations appear through time. The base of the Cuddapah Supergroup is sourced exclusively from the Dharwar Craton. But through time, specifically during the deposition of the Nallamalai Group, the Bairenkonda and Cumbum Formations the main source of the sediments shifts to the east compatible with the rise of the Eastern Ghats orogen.

However, an alternative interpretation is possible, where the detrital zircons are all sourced from the Eastern Ghats to the east of the Cuddapah Basin. In this model, original sediments sourced from the Dharwar Craton would have been recycled during the Eastern Ghats orogeny before being finally deposited in the Cuddapah Basin. The complex tectonic evolution of the area of study, along with the long duration of the sedimentation, would be translated into a multi-stage history of sedimentation.

*Basin Evolution*

The Cuddapah Supergroup was mostly deposited in a shallow marine environment. The base of the sequence appears to be deposited in an alluvial fan to fluvial environment; the rest of the sequence is interpreted as various marine environments. The Cuddapah Supergroup starts with the Papaghni Group consisting of conglomerates and medium to coarse grained sandstones progressing into shales and dolomitic carbonates followed by a break in sedimentation represented by an

unconformity. This is followed by the Chitravati Group comprising coarse to medium grained sandstones developing into shales, dolomitic carbonates and limestones followed by a unconformity. The Nallamalai Group follows with medium sandstones and at least one volcaniclastic layer progressing into shales and concluding with an unconformity. This sequence can be separated into three clear cycles of coarse to medium grained sandstones progressing into interbedded shales and dolomites ending with an unconformity. This pattern of sediments suggests a cyclicity in depositional setting, starting with shallow marine then a transgression to deeper waters followed by a break in sedimentation.

The age data from this study and previous studies suggests the Cuddapah Basin is not a foreland basin caused by the formation of the Eastern Ghats, as deposition of the Cuddapah sediments started before ~1900 Ma. This is before the Ongole Domain of the Eastern Ghats - the region of the Eastern Ghats directly adjacent to the Cuddapah Basin (Fig. 1) - was deformed at ~1600 Ma (Upadhyay *et al.* 2009). There was a large igneous intrusion into the upper crust in the south western Cuddapah region of Dharwar Craton between 2400 and 2000 Ma (Chatterjee & Bhattacharji 2001). This intrusion would have caused uplift followed by subsidence and faulting, possibly the cause of the initiation of the basin. This intrusion could explain the gravity high in the south west region of the basin reported by Kaila *et al.* (1979). This may suggest the Cuddapah Basin developed as an intracratonic sag type basin resulting from thermal subsidence. Pandey *et al.* (1997) presented data that suggests a mafic dyke swarm, the Mahbubnagar swarm, was emplaced at ~ 2170 Ma. They suggest these dykes caused an episode of heating leading to crustal extension and fracturing which

resulted in the formation of the Cuddapah Basin. This timing fits in with the time constraints on deposition of the Gulcheru Formation.

The stratigraphy of the Cuddapah Supergroup is consistent with a series of cycles of thermal events, resulting in the heating of the crust and uplift, corresponding to a break of sedimentation, followed by cooling and subsidence corresponding to a stage of normal faulting and syn-rift sedimentation. (Chatterjee & Bhattacharji 2001). This history of events would explain the pattern of shallow to deep sediments terminating in an unconformity. The oriental edge of the Dharwar Craton records a succession of magmatic intrusions which may be indicators of this cyclic thermal event, coeval with the deposition of the Cuddapah Supergroup. Dykes and sills in the Vempalle Formation of the Papaghni Group and similar features in the Tadpatri Formation of the Chitrayati Group could be the consequence of two igneous events causing crustal heating and uplift causing the unconformities that follow these groups. Heating during the deposition of the Nallamalai Group may have been caused by extensive alkaline and acidic volcanic activity (Chatterjee & Bhattacharji 2001) as well as the emplacement of kimberlite dykes. The depositional areas may have shifted as a result of gravity induced faulting producing the isolation of post-Cuddapah Supergroup sub-basins.

As the Eastern Ghats was deformed and uplifted it would have affected the evolution of the basin. The sediments of the younger Nallamalai Group appear to have come from the Eastern Ghats and it is possible that lithospheric flexure due to the crustal thickening in the Eastern Ghats caused increased subsidence of the basin, particularly in the eastern part of the basin, adjacent to the Eastern Ghats, where the Nallamalai

Group sediments are found and the basin is deepest. This represents a foreland basin stage of evolution of the Cuddapah Basin. Deformation events in the Eastern Ghats may also be responsible for the crescent shape of the Cuddapah Basin. The folded Nallamalai Group sediments (Fig. 4) suggest deformation occurred after deposition of the sediments.

*Petroleum Potential*

Previous studies regarding the petroleum potential for the Cuddapah Basin have concluded that there are potential hydrocarbon reserves in the Cuddapah Basin (Prasanna *et al.* 2008, Kalpana *et al.* 2010). The Directorate General of Hydrocarbons (DGH), India have grouped the Cuddapah Basin under Category IV sedimentary basins of India  meaning the basin is potentially prospective, by having possible existence of hydrocarbons (Kalpana *et al.* 2010). Stromatolitic algae and bacteria have been identified as potential sources capable of generating petroleum (Kalpana *et al.* 2010). There are multiple stromatolitic carbonate rich sediments in the Cuddapah Basin (Vempalle Formation and Tadpatri Formation) that could potentially be source rocks for hydrocarbons. In a mine for road rock near Yagantipalle (15º18'59.7"N, 78º11'40.8"E) there was a 1.5 m thick black carbon rich shale observed in the Tadpatri Formation (Fig. 9). There are potentially much more carbon rich shales in the basin that have not been discovered yet. Bertram (2010) has identified carbonates in the younger Kurnool Group, stratigraphically above the Cuddapah Supergroup, that have oxygen and carbon isotopic values indicating deep marine deposition; this would provide a good environment for hydrocarbon accumulation. An understanding of the history of burial and uplift of the basin and heat flow in the area is important, as this would indicate when petroleum would have been generated. This would be crucial to

knowing if any hydrocarbons are still likely to be present, because if they were generated too long ago it is likely they would no longer be present due to leakage and dispersion. This study has contributed to increasing the understanding of the history of the basin.

Sandstones with high porosity are plentiful in the Cuddapah Basin and provide a good potential reservoir for petroleum. To the east of the basin sandstones of the Nallamalai Group have been folded (Fig. 4) and thrust over by high grade metamorphosed rocks of the Eastern Ghats, providing a good trap for potential accumulation. This large, deep thrust may also be a potential seal or migration path. Any studies focusing on finding reservoirs would therefore be best to concentrate on the eastern margin of the basin.

Shales make good seals due to their low porosity. Each sequence of sandstones in the Cuddapah Supergroup is overlain with shales which provide a potential stratigraphic seal for reservoirs within any of the sandstones. In the folded Nallamalai Group at the eastern side of the basin, shales of the Cumbum Formation cap thick sandstone beds of the Bairenkonda Formation. These are ideal stratigraphic and structural traps and represent a good target for petroleum exploration. There are also potential stratigraphic traps in the western part of the Cuddapah Basin; shale beds in the transition from the thick beds of sandstone of the Pulivendla Formation to the Tadpatri Formation are a good seal.

Kalpana *et al.* (2010) did a study looking for traces of hydrocarbons in surface soils of the Cuddapah Basin. Surface geochemical prospecting of hydrocarbons comprises

investigation of near surface soils/ sediments for occurrence of hydrocarbons that may indicate the location of subsurface petroleum reservoirs. The basic assumption of all near surface geochemical prospecting techniques is that the hydrocarbons migrate to the surface from the sub-surface petroleum accumulations through faults and fractures and leave their signatures in the near surface soils (Kalpana *et al.* 2010). The study found occurrences of $C_1$–$C_4$ (methane-$C_1$, ethane-$C_2$, propane-$C_3$ and butane-$C_4$, (Prasanna *et al.* 2008)) hydrocarbons, demonstrating that the Cuddapah Basin has hydrocarbon resource potential. Prasanna *et al.* (2008) also found evidence for hydrocarbon micro-seepage from the subsurface through their study, using a similar method to Kalpana *et al.* (2010), that is geo-microbial prospecting in the surface soils or sediments of the Cuddapah Basin, measuring levels of bacteria that exclusively use light gaseous hydrocarbons ($C_1$-$C_4$) as a carbon source. Prasanna *et al.* (2008) detected levels that suggested that hydrocarbon micro-seepage of subsurface origin is present in the basin and this together with other surface geochemical prospecting results (Kalpana *et al.* 2010) indicate that the area is worth visiting for conventional petroleum exploration.

The Cuddapah Basin shows evidence of some hydrocarbon leakage at the surface, indicating potential petroleum reserves in the basin. Porous sandstones throughout the basin provide a good reservoir. Shales, folds and the large thrust fault at the eastern margin of the basin give multiple potential seals and traps. There are no known source rocks but there are potential source rocks, with extensive stromatolitic carbonate layers present in both the Vempalle Formation and Tadpatri Formation. The eastern margin of the basin appears to be the best target for conventional petroleum exploration.

# Conclusion

Sequence stratigraphy shows that the Cuddapah Supergroup was deposited in a shallow marine environment. U-Pb zircon geochronology indicates deposition occurred for *c.* 986 million years starting in the Palaeoproterozoic and ending in the Neoproterozoic. Basin formation was caused by thermal subsidence related to thermal events during the Palaeoproterozoic. The uplift of the Eastern Ghats changed the shape and the evolution of the Cuddapah Basin, increasing subsidence along the eastern part of the basin. Samples contain detrital zircon cores that indicate that the Cuddapah Supergroup sediments were sourced from a predominantly Palaeoproterozoic to Mesoproterozoic source region compatible with the Dharwar Craton and the Eastern Ghats.

# Acknowledgements

of the Cuddapah Basin.  Thanks to Billy Reid for discussions about the Eastern Ghats and to the whole Honours 2010 class.  Thanks to my Mum and Dad for supporting me through the year and reading through my thesis.

# References

ANAND M., GIBSON S. A., SUBBARAO K. V., KELLEY S. P. & DICKEN A. P. 2003. Early Proterozoic melt generation processes beneath the intra-cratonic Cuddapah Basin, southern India. *Journal of Petrology* **44**, 2139-2171.

BARTLEY J. K., SEMIKHATOV M. A., KAUFMAN A. J., KNOLL A. H., POPE M. C. & JACOBSEN S. B. 2001. Global events across the Mesoproterozoic-Neoproterozoic boundary: C and Sr isotopic evidence from Siberia. *Precambrian Research* **111**, 165-202.

BASKAR RAO Y. J., PANTULU G. V. C., DAMODARA REDDY V. & GOPALAN K. 1995. Time of early sedimentation and volcanism in the Proterozoic Cuddapah Basin, South India; evidence from the Rb-Sr age of Pulivendla mafic sill. *Memoir Geological Society of India* **33**, 329-338.

BERTRAM C. N. 2010. Sedimentology, Age and Stable Isotope Evolution of the Kurnool Group, India. *Unpublished.*

CHADWICK B., VASUDEV V. N. & HEGDE G. V. 2000. The Dharwar craton, southern India, interpreted as the result of Late Archaean oblique convergence. *Precambrian Research* **99**, 91-111.

CHAKRABARTI G., SHOME D., BAULUZ B. & SINHA S. 2009. Provenance and weathering history of Mesoproterozoic clastic sedimentary rocks from the basal Gulcheru Formation, Cuddapah Basin. *Journal of the Geological Society of India* **74**, 119-130.

CHALAPATHI RAO N. V., MILLER JOHN A., PYLE DAVID M. & MADHAVAN V. 1996. New Proterozoic K-Ar ages for some kimberlites and lamproites from the Cuddapah Basin and Dharwar Craton, South India; evidence for non-contemporaneous emplacement. *Precambrian Research* **79**, 3-4.

CHATTERJEE N. & BHATTACHARJI S. 2001. Petrology, geochemistry and tectonic settings of the mafic dikes and sills associated with the evolution of the Proterozoic Cuddapah Basin of south India. *Proceedings of the Indian Academy of Sciences-Earth and Planetary Sciences* **110**, 433-453.

CHAUDHURI A. K., SAHA D., DEB G. K., DEB S. P., MUKHERJEE M. K. & GHOSH G. 2002. The Purana basins of southern cratonic province of India - A case for mesoproterozoic fossil rifts. *Gondwana Research* **5**, 23-33.

CRAIG H. 1957. Isotopic standards for Carbon and Oxygen and correction factors for mass-spectrometric analysis of carbon dioxide. *Geochimica Et Cosmochimica Acta* **12**, 133-149.

CRAWFORD A. R. & COMPSTON W. 1973. The age of the Cuddapah and Kurnool Systems, southern India. *Journal of the Geological Society of Australia* **4**, 453-464.

DASGUPTA P. K. & BISWAS A. 2006. *Rhythms in Proterozoic Sedimentation : An Example From Peninsular India*. Satish Serial Publishing House, Delhi.

DASGUPTA P. K., BISWAS A. & MUKHERJEE R. 2005. 11. Cyclicity in paleoproterozoic to neoproterozoic cuddapah supergroup and its significance in basinal evolution. *In:* Jannes M. M. & Virgnio H. N. eds., *Developments in Sedimentology*, Vol. 57, pp 313-354, Elsevier.

DOBMEIER C. J. & RAITH M. M. 2003. Crustal architecture and evolution of the Eastern Ghats Belt and adjacent regions of India. *Geological Society Special Publications* **206**, 145-168.

FRENCH J. E., HEAMAN L. M., CHACKO T. & SRIVASTAVA R. K. 2008. 1891-1883 Ma Southern Bastar-Cuddapah mafic igneous events, India: A newly recognized large igneous province. *Precambrian Research* **160**, 308-322.

GRIFFIN W. L., PEARSON N. J., BELOUSOVA E., JACKSON S. E., VAN ACHTERBERGH E., O'REILLY S. Y. & SHEE S. R. 2000. The Hf isotope composition of cratonic mantle: LAM-MC-ICPMS analysis of zircon megacrysts in kimberlites. *Geochimica Et Cosmochimica Acta* **64**, 133-147.

HOU G. T., SANTOSH M., QIAN X. L., LISTER G. S. & LI J. H. 2008. Configuration of the Late Paleoproterozoic supercontinent Columbia: Insights from radiating mafic dyke swarms. *Gondwana Research* **14**, 395-409.

HOWARD K. E., HAND M., BAROVICH K. M., REID A., WADE B. P. & BELOUSOVA E. A. 2009. Detrital zircon ages; improving interpretation via Nd and Hf isotopic data. *Chemical Geology* **262**, 3-4.

JACKSON S. E., PEARSON N. J., GRIFFIN W. L. & BELOUSOVA E. A. 2004. The application of laser ablation-inductively coupled plasma-mass spectrometry to in-situ U/Pb zircon geochronology. *Chemical Geology* **211**, 47-69.

JAYANANDA M., MOYEN J. F., MARTIN H., PEUCAT J. J., AUVRAY B. & MAHABALESWAR B. 2000. Late Archaean (2550-2520 Ma) juvenile magmatism in the Eastern Dharwar craton, southern India: constraints from geochronology, Nd-Sr isotopes and whole rock geochemistry. *Precambrian Research* **99**, 225-254.

KAH L. C., SHERMAN A. G., NARBONNE G. M., KNOLL A. H. & KAUFMAN A. J. 1999. delta C-13 stratigraphy of the Proterozoic Bylot Supergroup, Baffin Island, Canada: implications for regional lithostratigraphic correlations. *Canadian Journal of Earth Sciences* **36**, 313-332.

KAILA K. L. & BHATIA S. C. 1981. Gravity study along the Kavali-Udipi Deep Seismic-Sounding profile in the Indian Peninsular Shield - Some inferences about the origin of anorthosites and the Eastern Ghats Orogeny *Tectonophysics* **79**, 129-143.

KAILA K. L., CHOWDHURY K. R., REDDY P. R., KRISHNA V. G., NARAIN H., SUBBOTIN S. I., SOLLOGUB V. B., CHEKUNOV A. V., KHARETCHKO G. E., LAZARENKO M. A. & ILCHENKO T. V. 1979. CRUSTAL STRUCTURE ALONG KAVALI-UDIPI PROFILE IN THE INDIAN PENINSULAR SHIELD FROM DEEP SEISMIC SOUNDING. *Journal of the Geological Society of India* **20**, 307-&.

KALPANA G., MADHAVI T., PATIL D. J., DAYAL A. M. & RAJU S. V. 2010. Light gaseous hydrocarbon anomalies in the near surface soils of Proterozoic Cuddapah Basin: Implications for hydrocarbon prospects. *Journal of Petroleum Science and Engineering* **73**, 161-170.

Ludwig K. R. 2003. *User's Manual for Isoplot 3.00*. Berkeley Geochronological Center, Special Publication No.4.

Manikyamba C., Kerrich R., Gonzalez-Alvarez I., Mathur R. & Khanna T. C. 2008. Geochemistry of Paleoproterozoic black shales from the Intracontinental Cuddapah basin, India: implications for provenance, tectonic setting, and weathering intensity. *Precambrian Research* **162**, 424-440.

Meijerink A. M. J., Rao D. P. & Rupke J. 1984. Stratigraphic and structural development of the Precambrian Cuddapah Basin, SE India. *Precambrian Research* **26**, 57-&.

Mezger K. & Cosca M. A. 1999. The thermal history of the Eastern Ghats Belt (India) as revealed by U-Pb and Ar-40/Ar-39 dating of metamorphic and magmatic minerals: implications for the SWEAT correlation. *Precambrian Research* **94**, 251-271.

Pandey B. K., Gupta J. N., Sarma K. J. & Sastry C. A. 1997. Sm---Nd, Pb---Pb and Rb---Sr geochronology and petrogenesis of the mafic dyke swarm of Mahbubnagar, South India: implications for Paleoproterozoic crustal evolution of the Eastern Dharwar Craton. *Precambrian Research* **84**, 181-196.

Prasanna M. V., Rasheed M. A. & Dayal A. M. 2008. Geo-microbial prospecting method for hydrocarbon exploration in Vengannapalli village, Cuddapah Basin, Andhra Pradesh, India. *Geochimica Et Cosmochimica Acta* **72**, A979-A979.

RIDING R. & SHARMA M. 1998. Late Palaeoproterozoic (~1800-1600 Ma) stromatolites, Cuddapah Basin, southern India: cyanobacterial or other bacterial microfabrics? *Precambrian Research* **92**, 21-35.

SAHA D. 2002. Multi-stage deformation in the Nallamalai Fold Belt, Cuddapah basin, South India - Implications for Mesoproterozoic tectonism along southeastern margin of India. *Gondwana Research* **5**, 701-719.

SEGAL I., HALICZ L. & PLATZNER I. T. 2003. Accurate isotope ratio measurements of ytterbium by multiple collection inductively coupled plasma mass spectrometry applying erbium and hafnium in an improved double external normalization procedure. *Journal of Analytical Atomic Spectrometry* **18**, 1217-1223.

SINGH A. P. & MISHRA D. C. 2002. Tectonosedimentary evolution of Cuddapah basin and Eastern Ghats mobile belt (India) as Proterozoic collision: gravity, seismic and geodynamic constraints. *Journal of Geodynamics* **33**, 249-267.

SLAMA J., KOSLER J., CONDON D. J., CROWLEY J. L., GERDES A., HANCHAR J. M., HORSTWOOD M. S. A., MORRIS G. A., NASDALA L., NORBERG N., SCHALTEGGER U., SCHOENE B., TUBRETT M. N. & WHITEHOUSE M. J. 2008. Plesovice zircon - A new natural reference material for U-Pb and Hf isotopic microanalysis. *Chemical Geology* **249**, 1-35.

UPADHYAY D., GERDES A. & RAITH M. M. 2009. Unraveling Sedimentary Provenance and Tectonothermal History of High-Temperature Metapelites, Using Zircon and Monazite Chemistry: A Case Study from the Eastern Ghats Belt, India. *Journal of Geology* **117**, 665-683.

VAN ACHTERBERGH E., RYAN C. G., JACKSON S. E. & GRIFFIN W. L. 2001. Data reduction software for LA-ICP-MS. *In:* Sylvester P. J. ed., *Laser-ablation-ICPMS in the earth sciences; principles and applications*, Vol. 29, pp 239-243, Mineralogical Association of Canada, Short Course Handbook, Ottowa.

VERVOORT J. D., PATCHETT P. J., SODERLUND U. & BAKER M. 2004. Isotopic composition of Yb and the determination of Lu concentrations and Lu/Hf ratios by isotope dilution using MC-ICPMS. *Geochemistry Geophysics Geosystems* **5**.

ZACHARIAH J. K., RAO Y. J. B., SRINIVASAN R. & GOPALAN K. 1999. Pb, Sr and Nd isotope systematics of uranium mineralised stromatolitic dolomites from the proterozoic Cuddapah Supergroup, south India: constraints on age and provenance. *Chemical Geology* **162**, 49-64.

# Figure Captions

*Figure 1* (a) Regional setting of the Cuddapah Basin, Dharwar Craton and Eastern Ghats, modified after French *et al* (2008); (b) Cuddapah Basin with sub-basins representing stratigraphic groups. The locations of the three sections are shown. Modified after Anand *et at.* (2003).

*Figure 2* Stratigraphy of the Cuddapah Supergroup with previous ages and ages from this study. Modified after Manikyamba *et al.* (2008) and Murphy (1979) originally based on King (1872).

*Figure 3* Space-time plot showing major tectonothermal events affecting the Dharwar Craton and Eastern Ghats regions with events located exclusively in the Ongole Domain outlined. All events are possible sources of detrital zircons found in the Cuddapah Basin. Events: (a) volcano-sedimentary greenstone belts, Sargur Group (Chadwick *et al.* 2000); (b) tonalitic–trondhjemitic–granodioritic basement (Jayananda *et al.* 2000); (c) volcano-sedimentary greenstone belts, Dharwar Supergroup (Chadwick *et al.* 2000), (Jayananda *et al.* 2000) (d) calc-alkaline to potassium rich granitic intrusions (Jayananda *et al.* 2000); (e) the Mahbubnagar mafic dyke swarm (Pandey *et al.* 1997); (f) large igneous province spanning the Bastar Craton, the Dharwar Craton and the Cuddapah Basin (French *et al.* 2008); (g) period of felsic magmatism (Dobmeier & Raith 2003); (h) felsic plutonic intrusion (Upadhyay *et al.* 2009); (i) ultra-high temperature metamorphic and deformation event (Upadhyay *et al.* 2009); (j) ductile brittle deformation associated with Mesoproterozoic rifting along the margin of Proto-India (Upadhyay *et al.* 2009); (k) partial melting event (Upadhyay *et al.* 2009); (l) thermal event (Upadhyay *et al.* 2009); (m) orogenic event associated with the assembly of the supercontinent Rodinia (Mezger & Cosca 1999) (Upadhyay *et al.* 2009); (n) orogenic event associated with assembly of the supercontinent Gondwana (Mezger & Cosca 1999), (Upadhyay *et al.* 2009).

*Figure 4* Cross section created using formation boundaries from Meijerink *et al.* (1984)'s map and observations in the field showing the Cuddapah Basin from point A to B on Figure 1, two interpretations of structures at depth are shown: (a) scenario one with deep thrust fault cutting off Nallamalai fold belt; (b) scenario two, all formations continue across the basin with no major interruptions.

*Figure 5* Graphs showing Hf isotope data (a) ages from U-Pb zircon geochronological analysis against epsilon Hf, blue points are from Gulcheru Formation, purple points are from Bairenkonda Formation (b) 176Hf/177Hf vs 176Yb/177Hf ratios for four zircon grains, Each point on the graph is one measurement (0.232 seconds) during the analysis, blue points are JM_Hf_01_15, red points are JM_Hf_01_30, green points are JM_Hf_01_30_Initial, purple points are JM_Hf_01_33, yellow points are JM_Hf_01_37.

*Figure 6* Photographs of sediments and sedimentary features of the Gulcheru Formation: (a) basal facies of Gulcheru Formation showing conglomerate beds; (b) cross-bedding; (c) trough bedding; (d) contact between basement rock and Gulcheru Formation; (e) channel filled with conglomerate sediments; (f) conglomerate beds.

*Figure 7* Photographs of sediments and sedimentary features of the Vempalle Formation: (a) mudcracks in fine grained sandstone; (b) dolomite and shale beds; (c) stromatolite in a laminated dolomite bed; (d) grainstone beds made of broken stromatolite, ooids and oncoids; (e) chert bed capping stromatolitic dolomite layer; (f) purple shales.

*Figure 8* Photographs of sediments and sedimentary features of the Pulivendla Formation: (a) cross-bedding; (b) mudcracks; (c) symmetrical ripples.

*Figure 9* Photographs of sediments and sedimentary features of the Tadpatri Formation: (a) stromatolite within a dolomite bed; (b) intermediate sill showing

contact with shales of the Tadpatri Formation below and above; (c) black carbon rich shale layer; (d) grey laminated dolomite; (e) beach rosette in dolomite layer interbedded with thin chert layers; (f) angular unconformity between Tadpatri Formation (bottom) and Banaganapalle Formation (above) of the Kurnool Group.

*Figure 10* Photographs of sediments and sedimentary features of the Gandikota Formation: (a) bedded medium grained sandstone; (b) sandstone concretions; (c) conjugate quartz veins; (d) cross-bedding.

*Figure 11* Photographs of sediments and sedimentary features of the Bairenkonda Formation: (a) fine to medium grained sandstone showing cross-bedding (b) coarse grained sandstone; (c) massive thickly bedded sandstone near to top contact of the formation (d) bar migration; (e) adhesion ripples; (f) symmetrical ripples.

*Figure 12* Photographs of sediments and sedimentary features of the Cumbum Formation: (a) transition from the Bairenkonda Formation to the Cumbum Formation, sandstones with thin shale beds; (b) shales near the base of the formation; (c) grey shales; (d) stretched tabular clasts of limestone within shale beds.

*Figure 13* Stratigraphic log of the Gulcheru Formation and the base of the Vempalle Formation. The position of geochronological sample CU10-01 is shown with maximum depositional age (1σ error). Total, Potassium, Uranium and Thorium columns show results from analysis by portable gamma ray spectrometer. Palaeocurrent column shows summary of palaeocurrent data collected.

*Figure 14* Stratigraphic log of a section of the Pulivendla Formation and a section of the Tadpatri Formation. The position of geochronological sample CU10-19 is shown with maximum depositional age (1σ error). Key for sedimentary structures and facies descriptions is given in Figure 13. Total, Potassium, Uranium and Thorium columns show results from analysis by portable gamma ray spectrometer. Palaeocurrent column shows summary of palaeocurrent data collected.

*Figure 15* Stratigraphic log comprising sections of the Bairenkonda Formation and the base of the Cumbum Formation.. The position of geochronological samples CU10-10 and CU10-21 are shown with maximum depositional age (1σ error). Key for sedimentary structures and facies descriptions is given in Figure 13. Total, Potassium, Uranium and Thorium columns show results from analysis by portable gamma ray spectrometer. Palaeocurrent column shows summary of palaeocurrent data collected.

*Figure 16* Sample CU10-01 LAICPMS U-Pb geochronological data for detrital zircons; (a) Conventional U-Pb concordia plot for all zircon ages with youngest analysis with concordancy greater than 90% and less than 110% labelled. Inset: Concordia plot for zircons with concordancy greater than 90% and less than 110%; (b) Relative probability distribution for all zircon ages – light blue and for zircons with concordancy greater than 90% and less than 110% - dark blue, peaks are labelled; (c) Cathodoluminescence image of a representative zircon from sample CU10-01.

*Figure 17* Sample CU10-19 LAICPMS U-Pb geochronological data for detrital zircons; (a) Conventional U-Pb concordia plot for all zircon ages with youngest analysis with concordancy greater than 90% and less than 110% labelled. Inset: Concordia plot for zircons with concordancy greater than 90% and less than 110%; (b) Relative probability distribution for all zircon ages – light blue and for zircons with concordancy greater than 90% and less than 110% - dark blue, peaks are labelled; (c) Cathodoluminescence image of a representative zircon from sample CU10-19.

*Figure 18* Sample CU10-10 LAICPMS U-Pb geochronological data for detrital zircons; (a) Conventional U-Pb concordia plot for all zircon ages with youngest analysis with concordancy greater than 90% and less than 110% labelled. Inset: Concordia plot for zircons with concordancy greater than 90% and less than 110%; (b) Relative probability distribution for all zircon ages – light blue and for zircons with concordancy greater than 90% and less than 110% - dark blue, peaks are labelled; (c) Cathodoluminescence image of a representative zircon from sample CU10-10.

*Figure 19* Sample CU10-21 LAICPMS U-Pb geochronological data for detrital zircons; (a) Conventional U-Pb concordia plot for all zircon ages with youngest analysis with concordancy greater than 90% and less than 110% labelled. Inset: Concordia plot for zircons with concordancy greater than 90% and less than 110%; (b) Relative probability distribution for all zircon ages – light blue and for zircons with concordancy greater than 90% and less than 110% - dark blue, peaks are

labelled; (c) Cathodoluminescence image of a representative zircon from sample CU10-21.

# List of Tables

*Table 1* Summary of age data collected from the Cuddapah Basin; previous work and from this study.

*Table 2* U-Pb zircon LAICPMS data for samples CU10-01, CU10-19, CU10-10 and CU10-21.

*Table 3* Hf isotope data for samples CU10-01 and CU10-19.

*Table 4* Stable isotope data for samples T1 and T2 from the Tadpatri Formation and V1 from the Vempalle Formation.
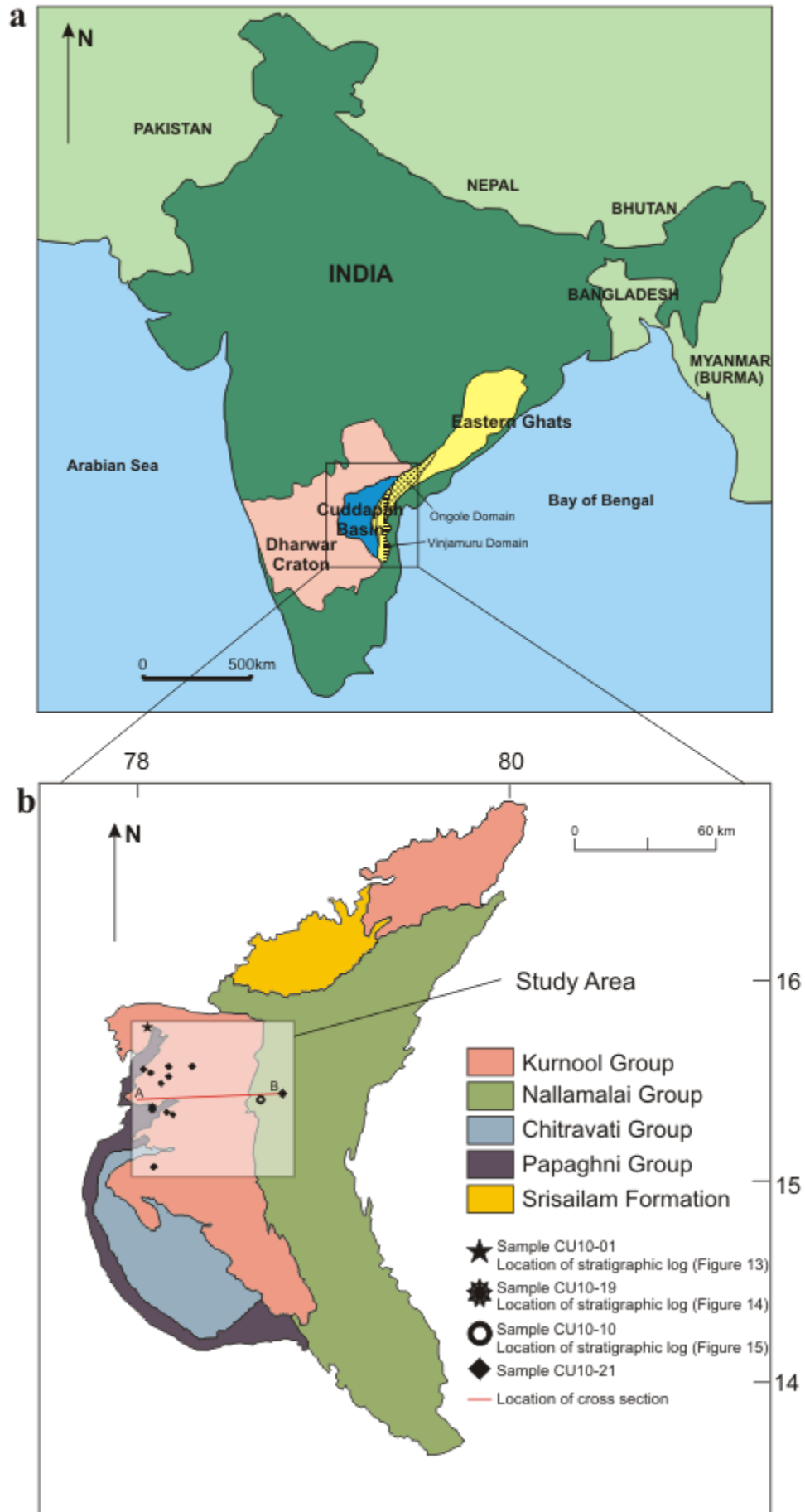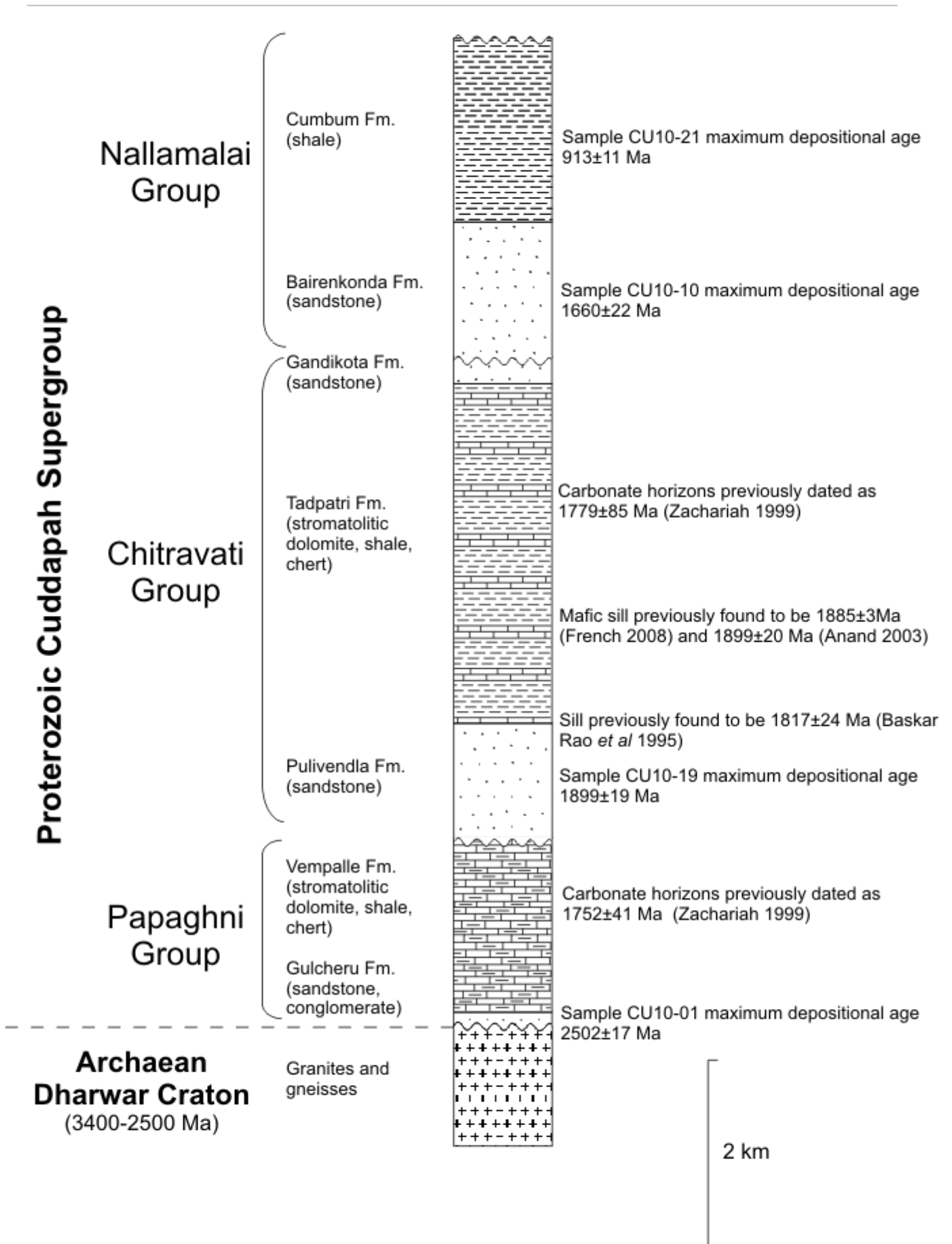
## Figures



Figure 1

Figure 2

Figure 3

Figure 4

Legend:
- Kurnool Group
- Cumbum Formation
- Bairenkonda Formation
- Tadpatri Formation
- Pulivendla Formation
- Vempalle Formation
- Gulchery Formation
- Basement Dharwar rocks
- Fault
- Eroded Sediments
- Formation Boundaries
- Current Topography
- Dip
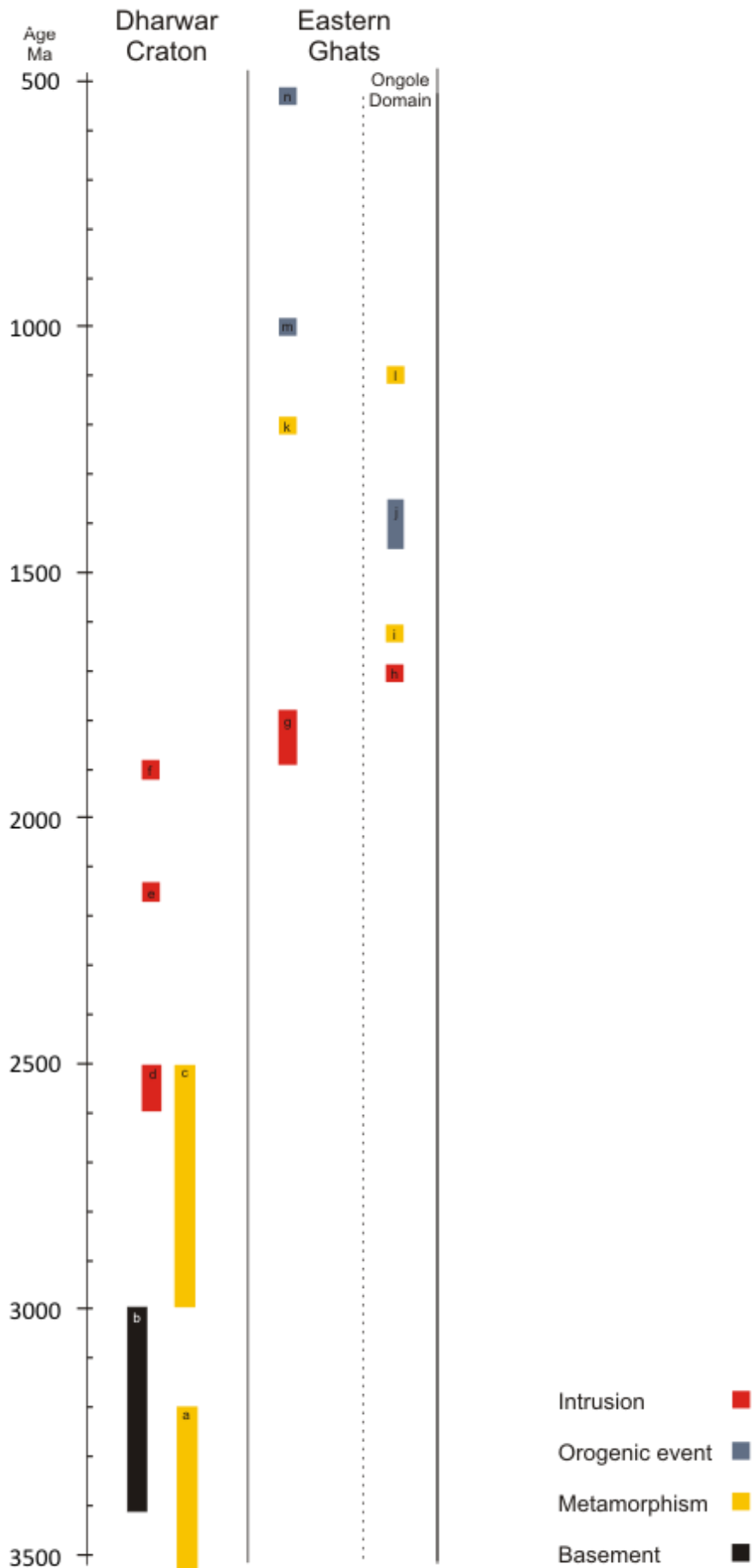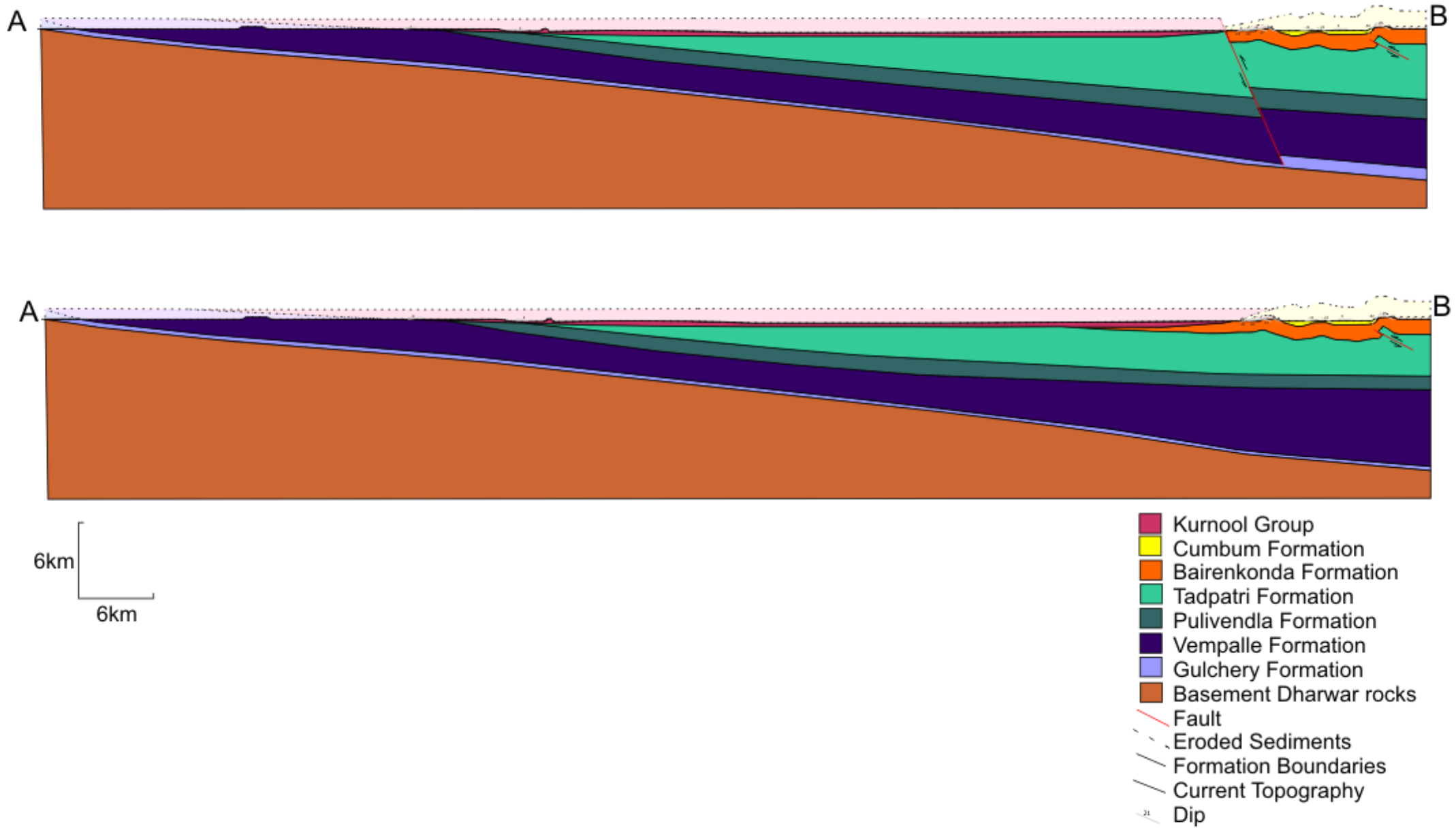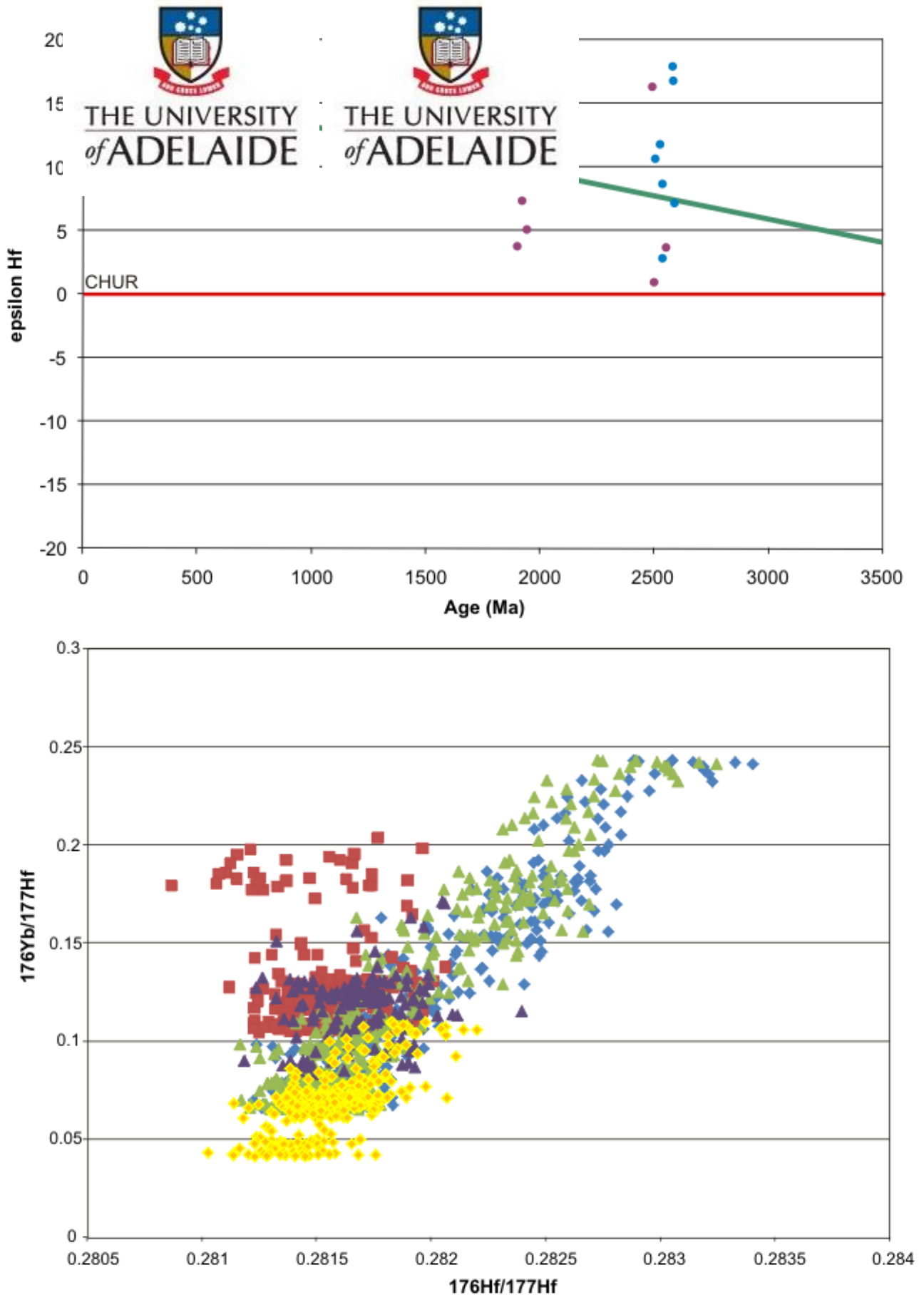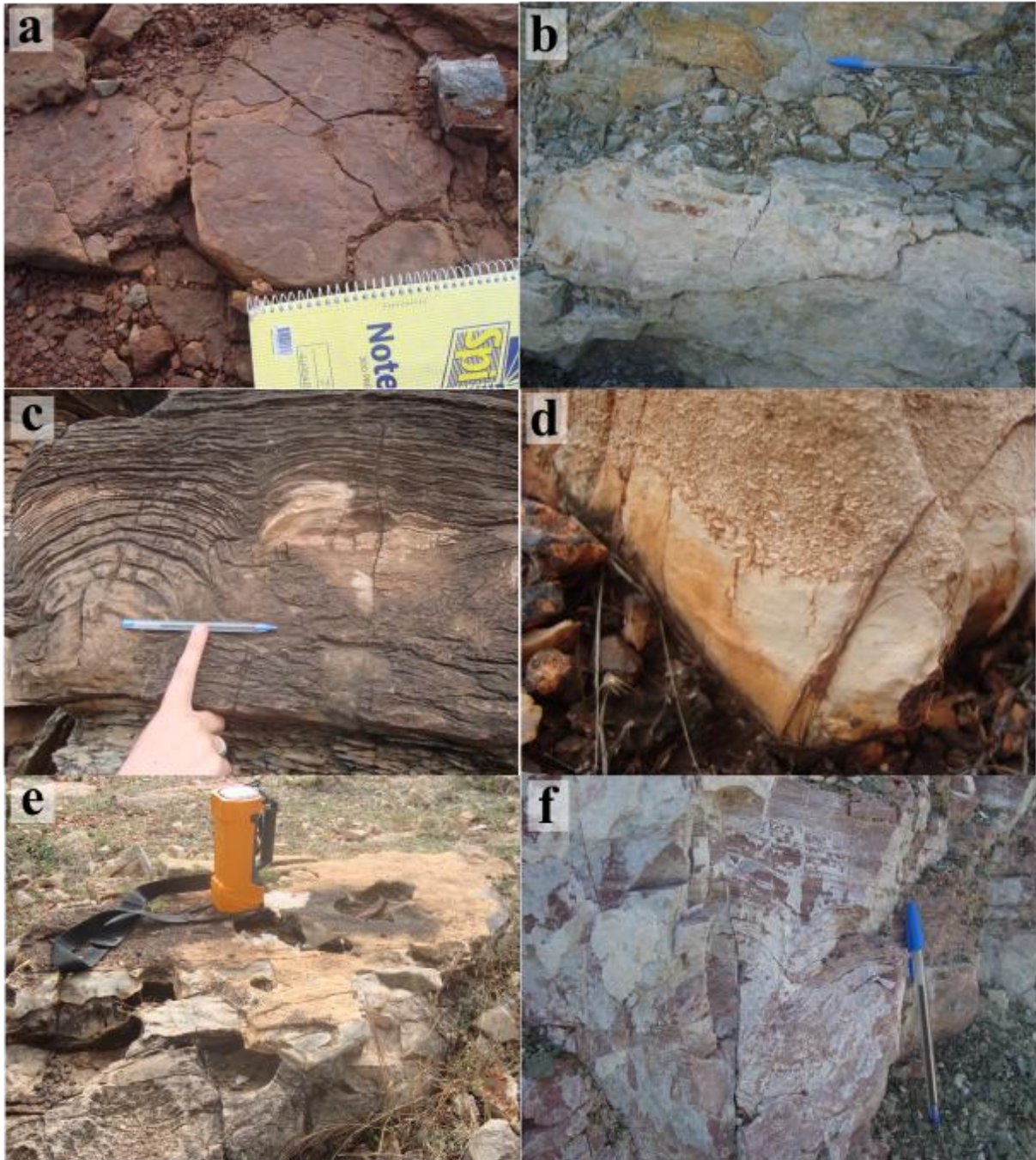
Figure 5

Figure 6

Figure 7

Figure 8

Figure 9
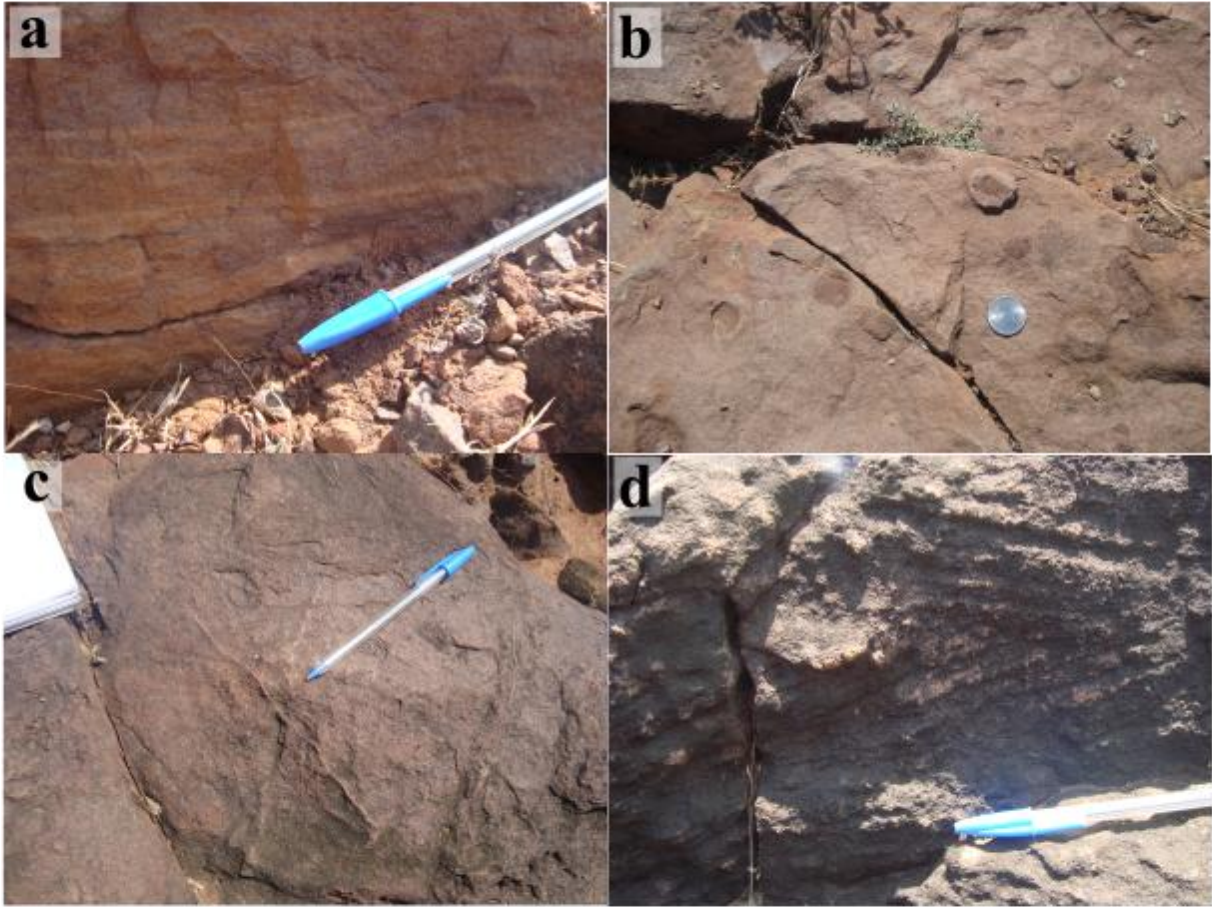
Figure 10

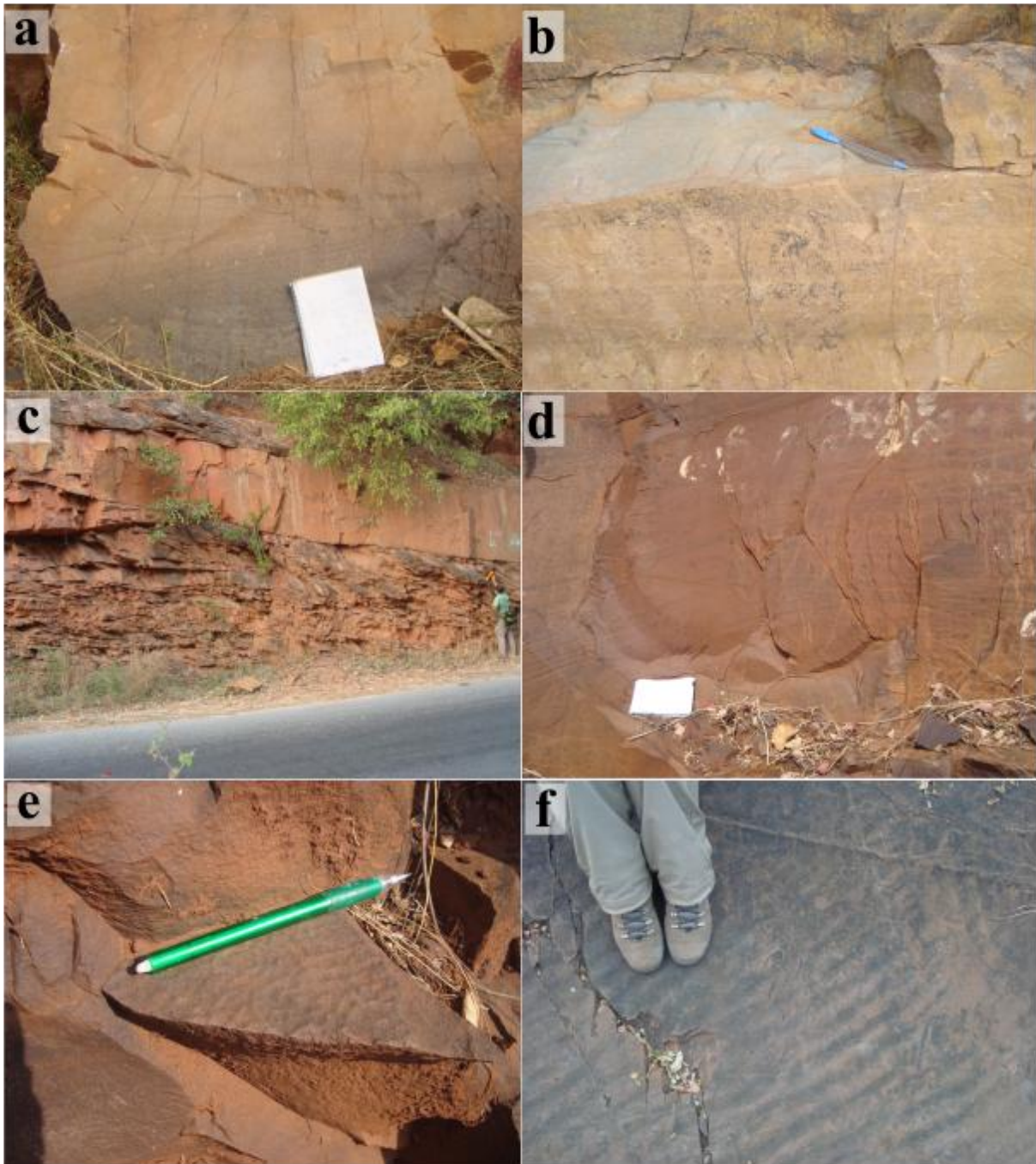Figure 11

Figure 12
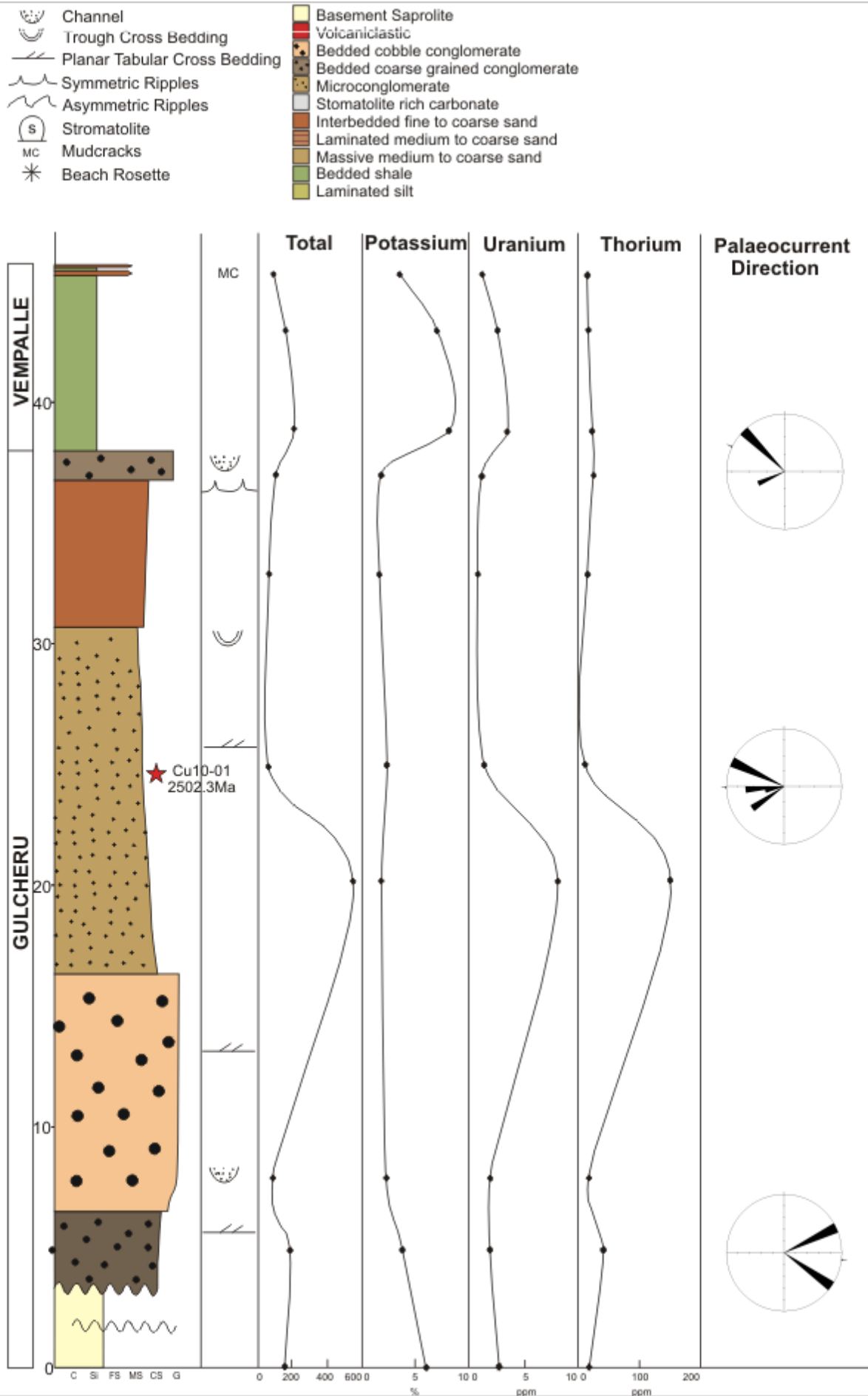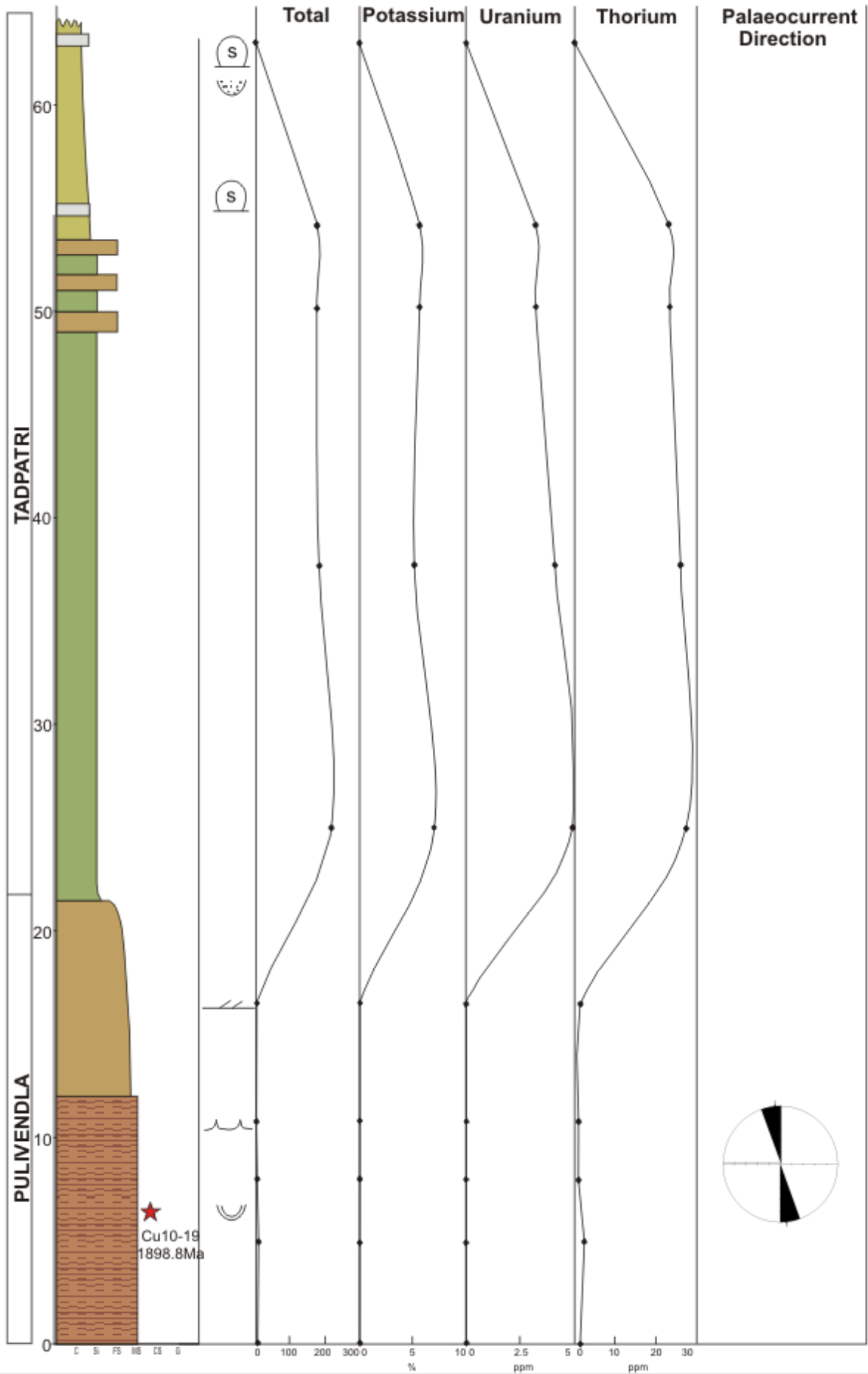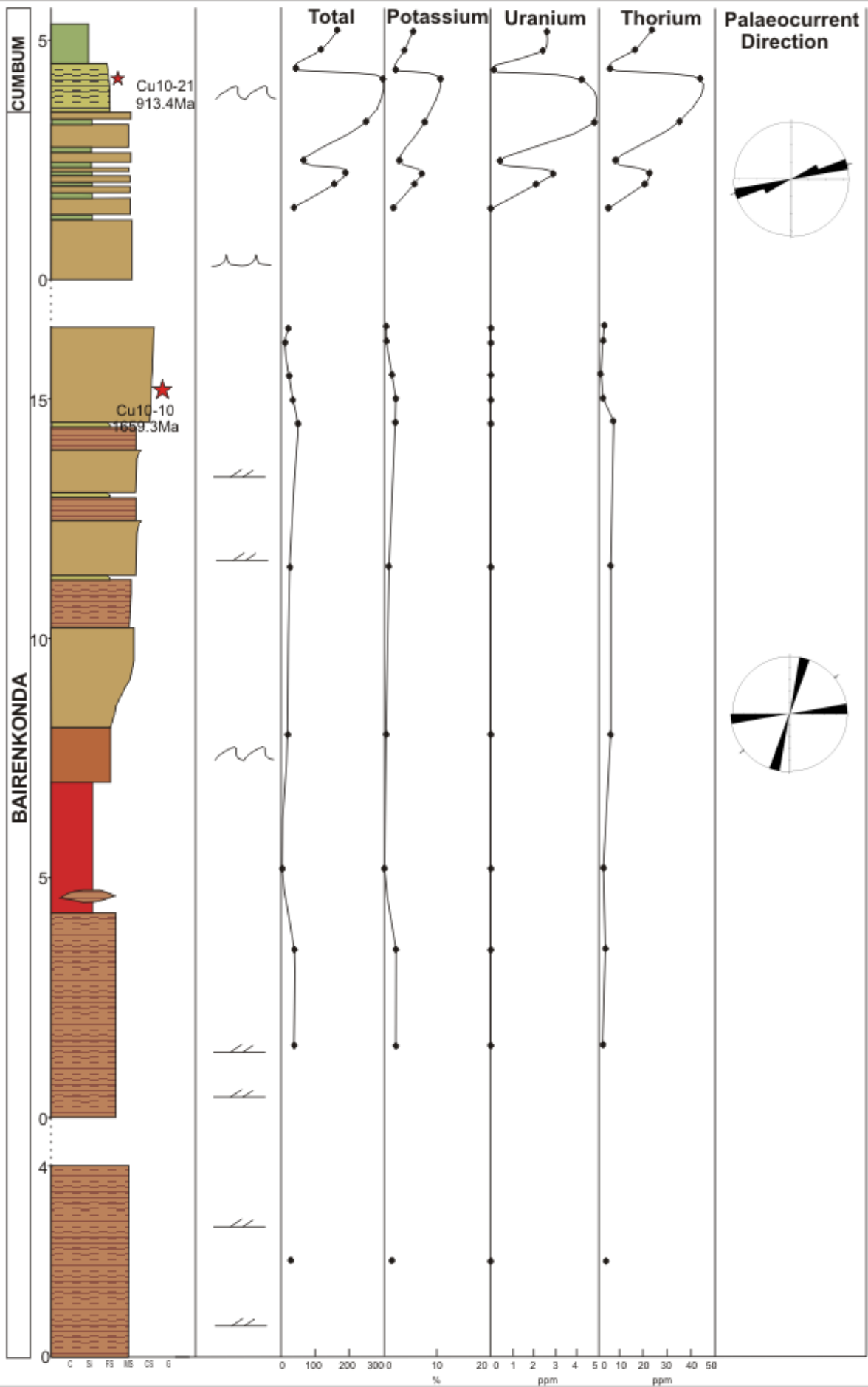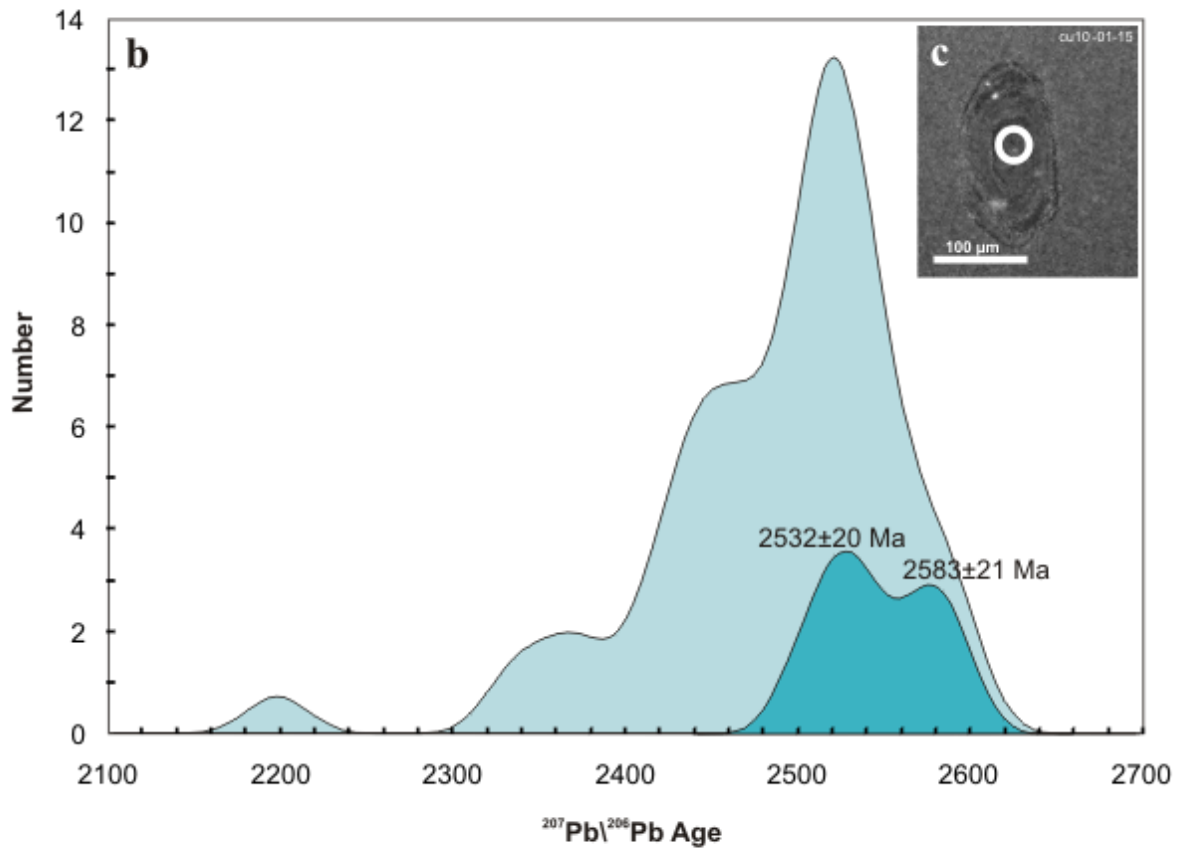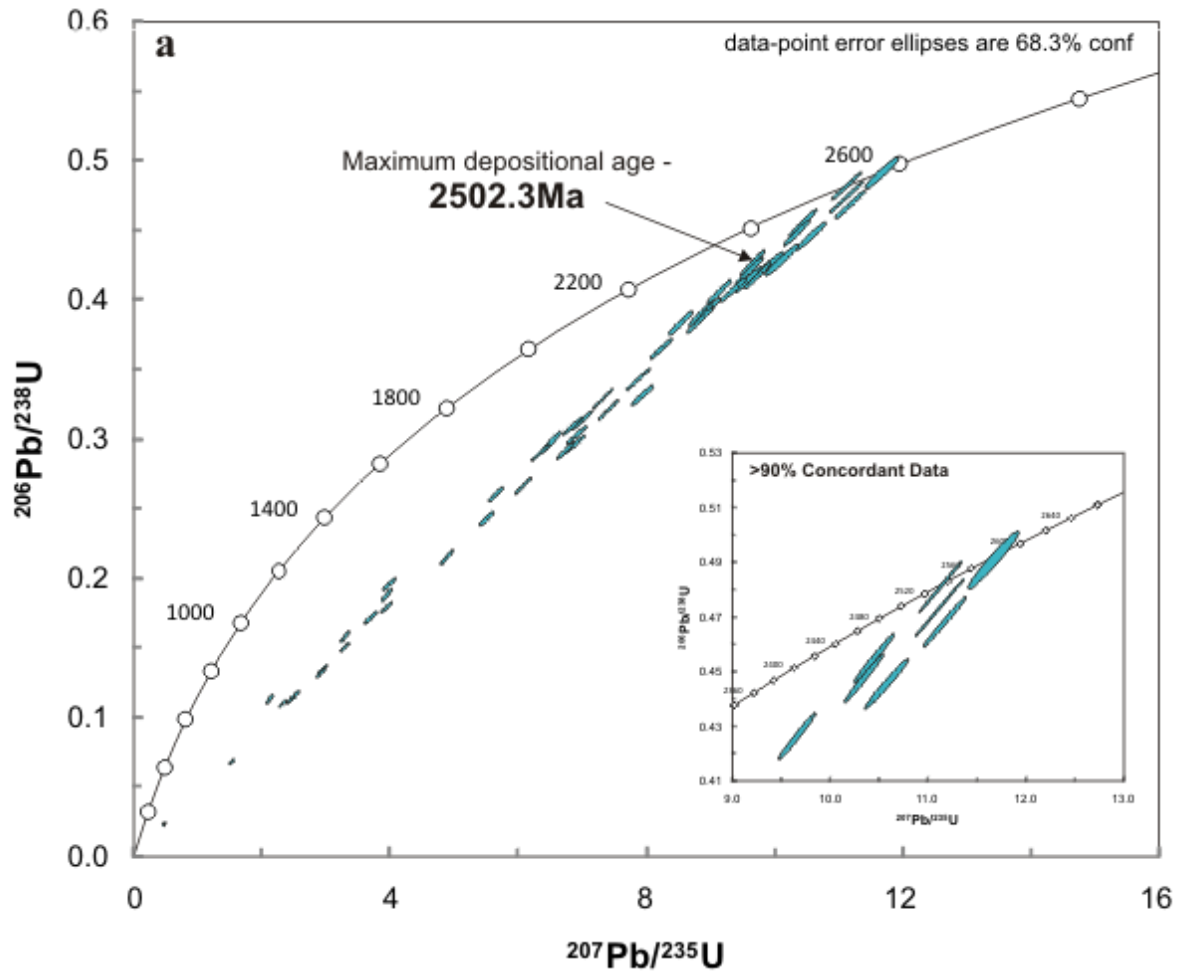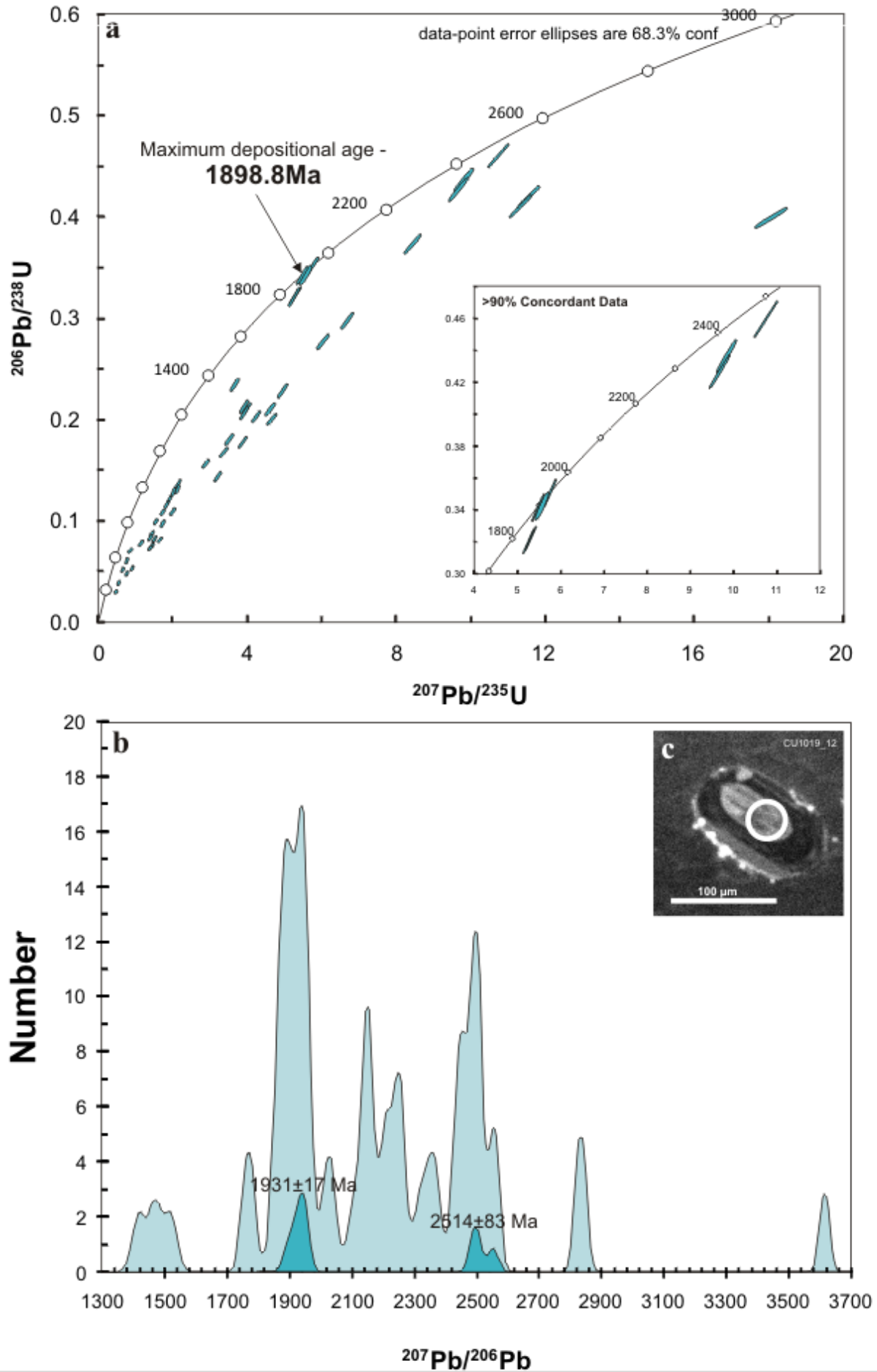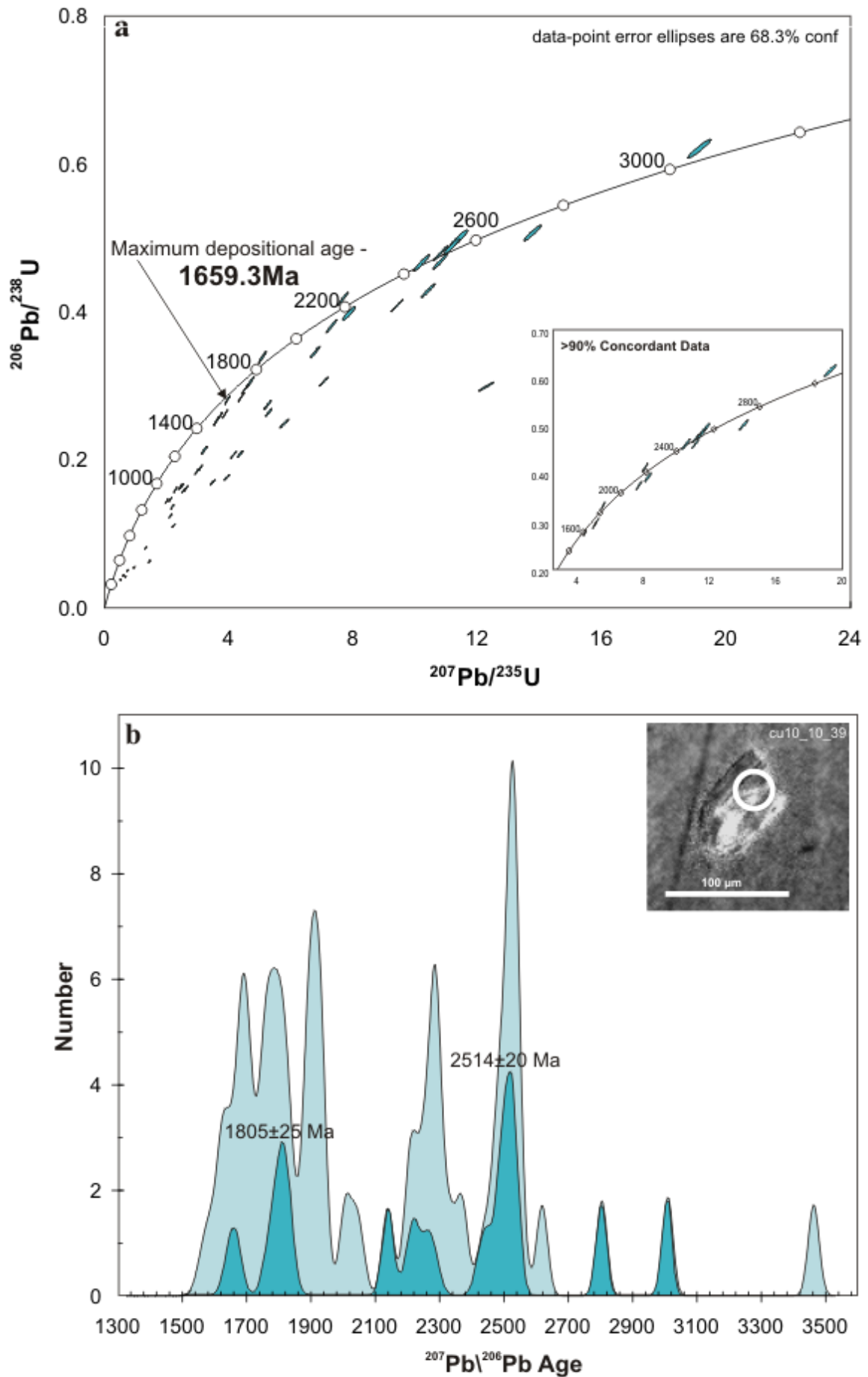
Figure 13

Figure 14

Figure 15

Figure 16
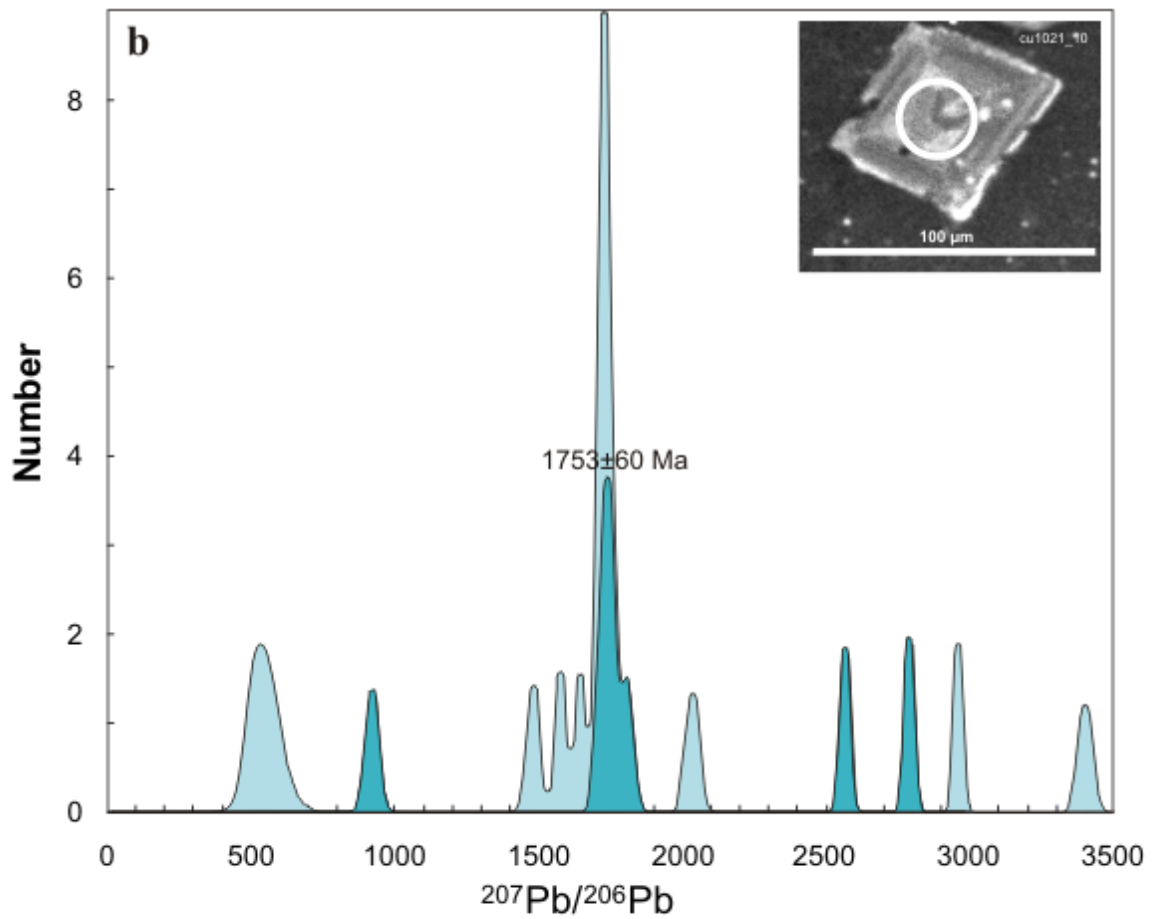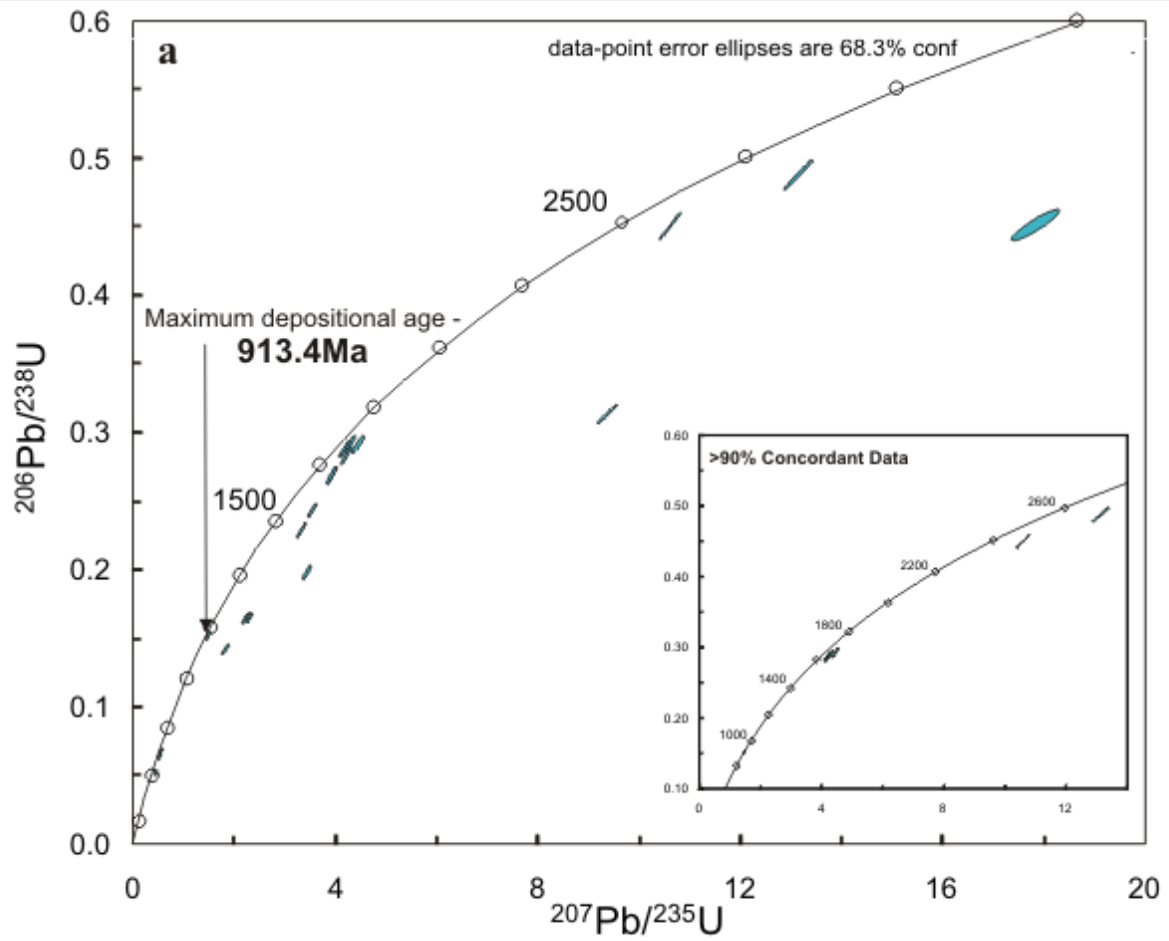
Figure 17

Figure 18

Figure 19

# Tables

| Formation | Dating Method | Age in Ma | Reference |
|---|---|---|---|
| Cumbum | U-Pb on zircons from sandstone | 913±11 | This study |
| Bairenkonda | Rb-Sr on intruded Kimberlite | 1200 | Crawford and Compston (1973) |
| | K-Ar on intruded Kimberlite | 1350±52 | Rao *et al.* (1996) |
| | U-Pb on zircons from sandstone | 1660±22 | This study |
| Tadpatri | $^{206}$Pb-$^{204}$Pb on U-mineralized carbonate | 1779±85 | Zachariah (1999) |
| | U-Pb on mafic sill | 1885±3 | French (2008) |
| | $^{40}$Ar-$^{39}$Ar on mafic sill | 1899±20 | Anand (2003) |
| Pulivendla | Rb–Sr on sill | 1817±24 | Baskar Rao *et al.* (1995) |
| | U-Pb on zircons from sandstone | 1899±19 | This study |
| Vempalle | $^{206}$Pb-$^{204}$Pb on U-mineralized carbonate | 1752±41 | Zachariah (1999) |
| Gulcheru | U-Pb on zircons from sandstone | 2502±17 | This study |

Table 1

| CU10-01 | Isotope Ratios | | | | | | | | | Ages Ma | | | | | | | | Conc. (%) | Age |
|---|---|---|---|---|---|---|---|---|---|---|---|---|---|---|---|---|---|---|---|
| Spot | $Pb^{207}/Pb^{206}$ | ±1 | $Pb^{206}/U^{238}$ | ±1 | $Pb^{207}/U^{235}$ | ±1 | $Pb^{208}/Th^{232}$ | ±1 | Rho | $Pb^{207}/Pb^{206}$ | ±1 | $Pb^{206}/U^{238}$ | ±1 | $Pb^{207}/U^{235}$ | ±1 | $Pb^{208}/Th^{232}$ | ±1 | | |
| cu10_01_01c | 0.13769 | 0.00147 | 0.11185 | 0.00176 | 2.12423 | 0.03291 | 0.01193 | 0.00014 | 0.984577 | 2198.3 | 18.4 | 683.5 | 10.19 | 1156.7 | 10.7 | 239.8 | 2.76 | 31 | |
| cu10_01_02 | 0.14882 | 0.00152 | 0.19501 | 0.00288 | 4.00141 | 0.05793 | 0.03885 | 0.00047 | 0.980291 | 2332.4 | 17.36 | 1148.5 | 15.56 | 1634.5 | 11.76 | 770.3 | 9.11 | 49 | |
| cu10_01_23 | 0.15018 | 0.00166 | 0.02309 | 0.0051 | 0.47811 | 0.11427 | 0.00273 | 0.00086 | 0.924149 | 2348 | 17.91 | 147.2 | 1.82 | 396.8 | 4.16 | 55.2 | 0.59 | 6 | |
| cu10_01_42 | 0.15204 | 0.00161 | 0.15691 | 0.0014 | 3.28901 | 0.03001 | 0.01106 | 0.00014 | 0.97786 | 2369 | 17.3 | 939.6 | 11.24 | 1478.5 | 9.96 | 222.3 | 2.58 | 40 | |
| cu10_01_26 | 0.15281 | 0.00182 | 0.18678 | 0.00298 | 3.93468 | 0.07006 | 0.02354 | 0.00011 | 0.896035 | 2377.6 | 17.23 | 1103.9 | 12.86 | 1620.8 | 10.15 | 470.2 | 5.02 | 46 | |
| cu10_01_43 | 0.15556 | 0.0019 | 0.10863 | 0.00427 | 2.32982 | 0.1047 | 0.01065 | 0.00016 | 0.87914 | 2408 | 17.46 | 664.8 | 8.15 | 1221.4 | 9.15 | 214.1 | 2.72 | 28 | |
| cu10_01_06c | 0.15643 | 0.00163 | 0.17143 | 0.00262 | 3.69749 | 0.05541 | 0.00874 | 0.00011 | 0.980543 | 2417.5 | 17.63 | 1020 | 14.42 | 1570.8 | 11.98 | 175.8 | 2.15 | 42 | |
| cu10_01_06r | 0.15689 | 0.00166 | 0.11557 | 0.00178 | 2.50011 | 0.03768 | 0.00675 | 0.00008 | 0.978536 | 2422.4 | 17.84 | 705 | 10.27 | 1272.1 | 10.93 | 136 | 1.6 | 29 | |
| cu10_01_18 | 0.15796 | 0.00159 | 0.25954 | 0.0033 | 5.65184 | 0.07096 | 0.06196 | 0.00063 | 0.987448 | 2434 | 16.95 | 1487.5 | 16.9 | 1924 | 10.83 | 1215.1 | 11.97 | 61 | |
| CU10_01_34 | 0.15853 | 0.00173 | 0.11213 | 0.00342 | 2.45053 | 0.07813 | 0.00772 | 0.00028 | 0.956635 | 2440.1 | 17.68 | 685.1 | 8.39 | 1257.6 | 9.31 | 155.4 | 1.68 | 28 | |
| cu10_01_03 | 0.15867 | 0.00163 | 0.29807 | 0.00442 | 6.52076 | 0.0946 | 0.03931 | 0.00046 | 0.978338 | 2441.6 | 17.24 | 1681.7 | 21.97 | 2048.7 | 12.77 | 779.3 | 8.88 | 69 | |
| cu10_01_13 | 0.15887 | 0.00164 | 0.28986 | 0.00363 | 6.34991 | 0.0794 | 0.06271 | 0.00065 | 0.998469 | 2443.6 | 17.38 | 1640.8 | 18.16 | 2025.4 | 10.97 | 1229.3 | 12.43 | 67 | |
| CU10_01_36 | 0.1593 | 0.0017 | 0.1496 | 0.00588 | 3.28507 | 0.1336 | 0.01305 | 0.00128 | 0.96646 | 2448.3 | 17.42 | 898.7 | 10.72 | 1477.5 | 9.91 | 262 | 2.92 | 37 | |
| cu10_01_09 | 0.15998 | 0.00165 | 0.17866 | 0.00235 | 3.93995 | 0.05144 | 0.01024 | 0.0001 | 0.99259 | 2455.4 | 17.33 | 1059.7 | 12.83 | 1621.9 | 10.57 | 206 | 2.04 | 43 | |
| cu10_01_10 | 0.16024 | 0.0017 | 0.13361 | 0.00171 | 2.95088 | 0.03794 | 0.00759 | 0.00008 | 0.995431 | 2458.1 | 17.84 | 808.4 | 9.72 | 1395.1 | 9.75 | 152.9 | 1.67 | 33 | |
| cu10_01_40 | 0.16117 | 0.00175 | 0.13173 | 0.00587 | 2.92792 | 0.13296 | 0.00781 | 0.00116 | 0.981277 | 2468 | 17.74 | 797.7 | 10.03 | 1389.2 | 10.12 | 157.1 | 2.25 | 32 | |
| cu10_01_47 | 0.16131 | 0.00165 | 0.30832 | 0.00515 | 6.85756 | 0.11344 | 0.06495 | 0.00098 | 0.990355 | 2469.5 | 17.08 | 1732.4 | 19.87 | 2093.2 | 11.49 | 1271.9 | 14.38 | 70 | |
| cu10_01_48 | 0.16196 | 0.00077 | 0.38221 | 0.00129 | 8.53533 | 0.01197 | 0.08093 | 0.00106 | 0.415514 | 2476.2 | 17.07 | 2086.6 | 24.02 | 2289.7 | 12.08 | 1573 | 18.4 | 84 | |
| cu10_01_16 | 0.16202 | 0.0017 | 0.32777 | 0.00419 | 7.31937 | 0.09358 | 0.03236 | 0.00036 | 0.999851 | 2476.9 | 17.58 | 1827.6 | 20.34 | 2151.2 | 11.42 | 643.7 | 6.96 | 74 | |
| CU10_01_32 | 0.16222 | 0.00205 | 0.31289 | 0.00693 | 6.99682 | 0.16959 | 0.05231 | 0.00199 | 0.913781 | 2478.9 | 17.32 | 1754.9 | 19.9 | 2111 | 11.44 | 1030.5 | 10.99 | 71 | |
| cu10_01_17 | 0.16373 | 0.00165 | 0.40546 | 0.00521 | 9.15055 | 0.11612 | 0.07598 | 0.00078 | 0.987575 | 2494.6 | 16.91 | 2194.1 | 23.91 | 2353.2 | 11.62 | 1480.2 | 14.65 | 88 | |
| cu10_01_11 | 0.16374 | 0.00166 | 0.36408 | 0.00467 | 8.21854 | 0.1045 | 0.05196 | 0.00052 | 0.987972 | 2494.7 | 16.95 | 2001.5 | 22.06 | 2255.4 | 11.47 | 1023.8 | 10.01 | 80 | |
| cu10_01_15 | 0.16448 | 0.00166 | 0.42624 | 0.00548 | 9.66392 | 0.12265 | 0.09255 | 0.00096 | 0.987161 | 2502.3 | 16.92 | 2288.7 | 24.76 | 2403.3 | 11.68 | 1789 | 17.67 | 91 | 2502 |
| cu10_01_24 | 0.16497 | 0.00167 | 0.38904 | 0.00503 | 8.84817 | 0.11366 | 0.08085 | 0.00084 | 0.993529 | 2507.3 | 16.87 | 2118.4 | 23.67 | 2322.5 | 11.78 | 1571.5 | 16.1 | 84 | |
| cu10_01_04 | 0.16508 | 0.00177 | 0.3906 | 0.00617 | 8.89451 | 0.1377 | 0.04977 | 0.00057 | 0.976302 | 2508.4 | 17.9 | 2125.6 | 28.59 | 2327.2 | 14.08 | 981.7 | 11.03 | 85 | |
| CU10_01_31 | 0.16508 | 0.00168 | 0.2143 | 0.00405 | 4.87711 | 0.0901 | 0.01619 | 0.00057 | 0.977528 | 2508.4 | 17.08 | 1251.7 | 14.33 | 1798.3 | 10.54 | 324.7 | 3.65 | 50 | |
| cu10_01_27 | 0.16511 | 0.00167 | 0.24222 | 0.00086 | 5.51443 | 0.01934 | 0.00806 | 0.00004 | 0.987796 | 2508.7 | 18.47 | 1398.2 | 15.49 | 1902.8 | 10.92 | 162.3 | 2.3 | 56 | |
| cu10_01_28 | 0.16556 | 0.00076 | 0.06739 | 0.00129 | 1.53828 | 0.01198 | 0.00387 | 0.00108 | 0.406843 | 2513.2 | 16.91 | 420.4 | 5.18 | 945.8 | 7.74 | 78.1 | 0.81 | 17 | |
| CU10_01_35 | 0.1659 | 0.00165 | 0.26558 | 0.00191 | 6.07348 | 0.0482 | 0.02418 | 0.00015 | 0.957433 | 2516.7 | 17.42 | 1518.3 | 17.44 | 1986.4 | 11.22 | 483 | 5.55 | 60 | |
| cu10_01_41 | 0.16594 | 0.00155 | 0.41983 | 0.00202 | 9.6023 | 0.04206 | 0.06271 | 0.00013 | 0.910366 | 2517.1 | 17.57 | 2259.7 | 26.67 | 2397.4 | 12.73 | 1229.4 | 22.11 | 90 | 2517 |
| cu10_01_25 | 0.16598 | 0.00155 | 0.39176 | 0.00237 | 8.96441 | 0.04934 | 0.08025 | 0.00025 | 0.909807 | 2517.5 | 16.82 | 2131 | 23.28 | 2334.4 | 11.58 | 1560.2 | 15.66 | 85 | |

Table 2

| Spot | Pb207/Pb206 | ±1 | Pb206/U238 | ±1 | Pb207/U235 | ±1 | Pb208/Th232 | ±1 | Rho | Pb207/Pb206 | ±1 | Pb206/U238 | ±1 | Pb207/U235 | ±1 | Pb208/Th232 | ±1 | Conc.(%) | Age |
|---|---|---|---|---|---|---|---|---|---|---|---|---|---|---|---|---|---|---|---|
| cu10_01_39 | 0.16603 | 0.0017 | 0.30191 | 0.00176 | 6.91075 | 0.03916 | 0.04438 | 0.00011 | 0.972036 | 2518 | 17.08 | 1700.8 | 19.4 | 2100 | 11.44 | 877.7 | 9.96 | 68 | |
| cu10_01_05 | 0.16658 | 0.00179 | 0.38501 | 0.00557 | 8.84033 | 0.12721 | 0.06846 | 0.00094 | 0.994648 | 2523.6 | 17.96 | 2099.6 | 25.95 | 2321.7 | 13.13 | 1338.5 | 17.75 | 83 | |
| CU10_01_37 | 0.16666 | 0.00171 | 0.45475 | 0.00578 | 10.44747 | 0.13206 | 0.11682 | 0.00122 | 0.994501 | 2524.4 | 16.99 | 2416.3 | 26.05 | 2475.3 | 11.85 | 2233.1 | 23.08 | 96 | 2524 |
| cu10_01_21 | 0.16669 | 0.00172 | 0.40708 | 0.00554 | 9.35533 | 0.12671 | 0.08035 | 0.00074 | 0.995226 | 2524.7 | 16.87 | 2201.6 | 23.8 | 2373.5 | 11.59 | 1562.2 | 15.87 | 87 | |
| cu10_01_12 | 0.16671 | 0.00179 | 0.34253 | 0.00472 | 7.87164 | 0.10823 | 0.02373 | 0.00024 | 0.99779 | 2524.8 | 17.93 | 1898.8 | 22.65 | 2216.4 | 12.39 | 474 | 4.81 | 75 | |
| CU10_01_38 | 0.16771 | 0.00077 | 0.44736 | 0.00127 | 10.3425 | 0.01195 | 0.11208 | 0.00104 | 0.407001 | 2534.9 | 16.99 | 2383.5 | 25.72 | 2465.9 | 11.82 | 2147.2 | 22.14 | 94 | 2535 |
| CU10_01_30 | 0.16782 | 0.00169 | 0.48095 | 0.0027 | 11.12732 | 0.06098 | 0.1218 | 0.00018 | 0.976187 | 2536 | 17.54 | 2531.4 | 26.87 | 2533.8 | 11.98 | 2323.1 | 24.58 | 100 | 2536 |
| cu10_01_14 | 0.16795 | 0.0018 | 0.31971 | 0.0044 | 7.40264 | 0.1018 | 0.01639 | 0.00017 | 0.999228 | 2537.3 | 17.89 | 1788.3 | 21.5 | 2161.3 | 12.3 | 328.7 | 3.46 | 70 | |
| cu10_01_22 | 0.16797 | 0.00158 | 0.41389 | 0.00029 | 9.58374 | 0.00605 | 0.06926 | 0.00003 | 0.900964 | 2537.5 | 17.11 | 2232.7 | 25.24 | 2395.6 | 12.16 | 1353.5 | 14.02 | 88 | |
| CU10_01_29 | 0.16817 | 0.00177 | 0.29072 | 0.00617 | 6.74018 | 0.14303 | 0.02394 | 0.00136 | 0.999874 | 2539.5 | 17 | 1645.1 | 18.24 | 2077.9 | 11.02 | 478.1 | 5.36 | 65 | |
| cu10_01_20 | 0.16879 | 0.00168 | 0.29552 | 0.0052 | 6.87625 | 0.1182 | 0.02587 | 0.00085 | 0.976898 | 2545.7 | 17.27 | 1669 | 19.64 | 2095.6 | 11.75 | 516.2 | 5.67 | 66 | |
| cu10_01_07 | 0.16937 | 0.0018 | 0.42387 | 0.00647 | 9.89758 | 0.14878 | 0.08316 | 0.00104 | 0.984791 | 2551.4 | 17.7 | 2278 | 29.27 | 2425.3 | 13.86 | 1614.6 | 19.33 | 89 | |
| cu10_01_19 | 0.16954 | 0.00175 | 0.41676 | 0.00395 | 9.74115 | 0.09116 | 0.06656 | 0.00029 | 0.987377 | 2553.1 | 17 | 2245.8 | 24.46 | 2410.6 | 11.8 | 1302.4 | 13.24 | 88 | |
| cu10_01_08 | 0.17046 | 0.00189 | 0.47318 | 0.00701 | 11.11739 | 0.16453 | 0.06943 | 0.00097 | 0.998966 | 2562.1 | 18.44 | 2497.5 | 30.67 | 2533 | 13.79 | 1356.8 | 18.39 | 97 | 2562 |
| cu10_01_01 | 0.17107 | 0.00184 | 0.42814 | 0.00684 | 10.1067 | 0.15795 | 0.09638 | 0.00121 | 0.978228 | 2568.1 | 17.83 | 2297.3 | 30.9 | 2444.6 | 14.44 | 1859.8 | 22.28 | 89 | |
| cu10_01_45 | 0.17214 | 0.00177 | 0.44539 | 0.00607 | 10.57253 | 0.14384 | 0.10814 | 0.00141 | 0.99828 | 2578.6 | 18.39 | 2374.7 | 26.64 | 2486.3 | 12.63 | 2075.5 | 27.57 | 92 | 2579 |
| CU10_01_33 | 0.1725 | 0.00167 | 0.49077 | 0.00145 | 11.67135 | 0.03162 | 0.1218 | 0.00008 | 0.916961 | 2582.1 | 19.71 | 2574 | 29.96 | 2578.4 | 13.59 | 2311.8 | 35.94 | 100 | 2582 |
| cu10_01_46 | 0.17307 | 0.00164 | 0.46805 | 0.00403 | 11.16826 | 0.08889 | 0.11746 | 0.00076 | 0.924389 | 2587.6 | 16.97 | 2475 | 26.65 | 2537.3 | 12 | 2244.7 | 25.44 | 96 | 2588 |
| cu10_01_44 | 0.17421 | 0.00191 | 0.33098 | 0.00597 | 7.94894 | 0.14396 | 0.01088 | 0.00151 | 0.995956 | 2598.5 | 18.05 | 1843.1 | 20.67 | 2225.2 | 11.82 | 218.6 | 3.2 | 71 | |

| CU10-10 | Isotope Ratios | | | | | | | | | Ages Ma | | | | | | | | Conc. (%) | Age |
|---|---|---|---|---|---|---|---|---|---|---|---|---|---|---|---|---|---|---|---|
| Spot | Pb207/Pb206 | ±1 | Pb206/U238 | ±1 | Pb207/U235 | ±1 | Pb208/Th232 | ±1 | Rho | Pb207/Pb206 | ±1 | Pb206/U238 | ±1 | Pb207/U235 | ±1 | Pb208/Th232 | ±1 | | |
| cu10_10_18 | 0.09765 | 0.00127 | 0.03827 | 0.00058 | 0.51504 | 0.00797 | 0.00423 | 0.00008 | 0.979382 | 1579.7 | 24.09 | 242.1 | 3.6 | 421.8 | 5.34 | 85.3 | 1.54 | 15 | |
| cu10_10_41 | 0.09998 | 0.00113 | 0.04441 | 0.00062 | 0.61193 | 0.00861 | 0.00842 | 0.00015 | 0.992224 | 1623.6 | 20.94 | 280.1 | 3.81 | 484.8 | 5.42 | 169.6 | 2.95 | 17 | |
| cu10_10_17 | 0.10053 | 0.00114 | 0.14429 | 0.00206 | 1.99922 | 0.02858 | 0.02912 | 0.00032 | 0.998687 | 1633.9 | 20.93 | 868.9 | 11.63 | 1115.2 | 9.68 | 580.2 | 6.32 | 53 | |
| cu10_10_40 | 0.10192 | 0.00123 | 0.28099 | 0.00411 | 3.94892 | 0.05726 | 0.03128 | 0.00096 | 0.991339 | 1659.3 | 22.13 | 1596.4 | 20.69 | 1623.8 | 11.75 | 622.6 | 18.79 | 96 | 1659 |
| cu10_10_31 | 0.10334 | 0.0011 | 0.2522 | 0.00356 | 3.59375 | 0.04987 | 0.0503 | 0.00071 | 0.983075 | 1684.9 | 19.5 | 1449.8 | 18.32 | 1548.2 | 11.02 | 991.9 | 13.72 | 86 | |
| cu10_10_37 | 0.10348 | 0.00119 | 0.15934 | 0.00224 | 2.27318 | 0.03238 | 0.01343 | 0.00034 | 0.986916 | 1687.4 | 21.04 | 953.1 | 12.43 | 1204 | 10.05 | 269.6 | 6.68 | 56 | |
| cu10_10_04 | 0.1039 | 0.00109 | 0.25862 | 0.00342 | 3.70481 | 0.0484 | 0.0558 | 0.00058 | 0.987906 | 1694.9 | 19.16 | 1482.8 | 17.54 | 1572.4 | 10.45 | 1097.5 | 11.08 | 87 | |
| cu10_10_01 | 0.10464 | 0.00105 | 0.14693 | 0.00184 | 2.11968 | 0.02596 | 0.03886 | 0.0004 | 0.977973 | 1708 | 18.36 | 883.7 | 10.32 | 1155.2 | 8.45 | 770.6 | 7.79 | 52 | |
| cu10_10_26 | 0.1062 | 0.00136 | 0.05043 | 0.00068 | 0.73778 | 0.01074 | 0.01196 | 0.00017 | 0.926281 | 1733.8 | 23.24 | 317.2 | 4.15 | 561.1 | 6.27 | 240.2 | 3.42 | 18 | |
| cu10_10_47 | 0.10728 | 0.00114 | 0.26211 | 0.00352 | 3.87649 | 0.05202 | 0.02949 | 0.0005 | 0.999246 | 1753.6 | 19.27 | 1500.6 | 17.99 | 1608.8 | 10.83 | 587.4 | 9.73 | 86 | |
| cu10_10_28 | 0.10809 | 0.00117 | 0.16334 | 0.00234 | 2.43259 | 0.03446 | 0.01343 | 0.0002 | 0.988833 | 1767.4 | 19.62 | 975.3 | 12.97 | 1252.3 | 10.19 | 269.6 | 4.03 | 55 | |

Table 2

| | | | | | | | | | | | | | | | | | | | |
|---|---|---|---|---|---|---|---|---|---|---|---|---|---|---|---|---|---|---|---|
| cu10_10_20 | 0.10875 | 0.00137 | 0.33911 | 0.00499 | 5.08259 | 0.07712 | 0.06247 | 0.00093 | 0.969791 | 1778.5 | 22.8 | 1882.4 | 24.04 | 1833.2 | 12.87 | 1224.7 | 17.69 | 106 | 1779 |
| cu10_10_11 | 0.10912 | 0.00146 | 0.21347 | 0.00318 | 3.21004 | 0.05074 | 0.03021 | 0.00051 | 0.942432 | 1784.7 | 24.28 | 1247.3 | 16.87 | 1459.6 | 12.24 | 601.7 | 10.09 | 70 | |
| cu10_10_46 | 0.10981 | 0.00121 | 0.16442 | 0.00232 | 2.48816 | 0.03493 | 0.02729 | 0.00054 | 0.994917 | 1796.2 | 19.94 | 981.3 | 12.82 | 1268.6 | 10.17 | 544.3 | 10.68 | 55 | |
| cu10_10_05 | 0.11077 | 0.00123 | 0.2957 | 0.00404 | 4.51589 | 0.06236 | 0.06948 | 0.00083 | 0.989389 | 1812.1 | 20.02 | 1669.9 | 20.08 | 1733.9 | 11.48 | 1357.7 | 15.68 | 92 | 1812 |
| cu10_10_21 | 0.11143 | 0.00144 | 0.30556 | 0.00465 | 4.69285 | 0.0734 | 0.04336 | 0.00092 | 0.972965 | 1822.9 | 23.22 | 1718.8 | 22.94 | 1766 | 13.09 | 857.9 | 17.86 | 94 | 1823 |
| cu10_10_48 | 0.112 | 0.00122 | 0.2848 | 0.00393 | 4.39657 | 0.06069 | 0.05491 | 0.00095 | 0.999653 | 1832.1 | 19.6 | 1615.5 | 19.7 | 1711.7 | 11.42 | 1080.5 | 18.28 | 88 | |
| cu10_10_12 | 0.11534 | 0.00154 | 0.04247 | 0.00065 | 0.67538 | 0.01048 | 0.00395 | 0.00007 | 0.98632 | 1885.1 | 23.87 | 268.2 | 4.03 | 524 | 6.35 | 79.6 | 1.5 | 14 | |
| cu10_10_42 | 0.11588 | 0.00119 | 0.13682 | 0.0019 | 2.18559 | 0.02928 | 0.0167 | 0.00027 | 0.964714 | 1893.6 | 18.32 | 826.7 | 10.78 | 1176.5 | 9.33 | 334.8 | 5.34 | 44 | |
| cu10_10_23 | 0.1161 | 0.00121 | 0.15839 | 0.00222 | 2.53458 | 0.03461 | 0.03777 | 0.00049 | 0.97425 | 1897.1 | 18.62 | 947.8 | 12.36 | 1282 | 9.94 | 749.3 | 9.45 | 50 | |
| cu10_10_15 | 0.11699 | 0.00126 | 0.1841 | 0.00264 | 2.96723 | 0.04142 | 0.02374 | 0.00031 | 0.973439 | 1910.7 | 19.14 | 1089.3 | 14.36 | 1399.3 | 10.6 | 474.3 | 6.16 | 57 | |
| cu10_10_02 | 0.11787 | 0.00126 | 0.16138 | 0.00222 | 2.62217 | 0.03562 | 0.0439 | 0.00046 | 0.987483 | 1924.1 | 19.09 | 964.5 | 12.35 | 1306.9 | 9.98 | 868.4 | 8.92 | 50 | |
| cu10_10_14 | 0.11827 | 0.00123 | 0.18886 | 0.0026 | 3.07923 | 0.04149 | 0.0352 | 0.00041 | 0.978741 | 1930.2 | 18.45 | 1115.2 | 14.1 | 1427.5 | 10.33 | 697.7 | 7.94 | 58 | |
| cu10_10_25 | 0.11852 | 0.00123 | 0.08088 | 0.00118 | 1.32113 | 0.0184 | 0.00906 | 0.00013 | 0.954622 | 1934 | 18.48 | 501.4 | 7.05 | 855 | 8.05 | 182.2 | 2.69 | 26 | |
| cu10_10_27 | 0.1235 | 0.00127 | 0.12432 | 0.00179 | 2.11598 | 0.02923 | 0.0168 | 0.00017 | 0.959412 | 2007.4 | 18.14 | 755.4 | 10.28 | 1154 | 9.52 | 254.6 | 3.32 | 38 | |
| cu10_10_10 | 0.12619 | 0.00145 | 0.05478 | 0.00074 | 0.95289 | 0.0135 | 0.02502 | 0.00029 | 0.978874 | 2045.5 | 20.1 | 343.8 | 4.5 | 679.6 | 6.84 | 499.5 | 5.67 | 17 | |
| cu10_10_50 | 0.13312 | 0.00136 | 0.41794 | 0.00562 | 7.66936 | 0.1026 | 0.09359 | 0.00135 | 0.981875 | 2139.6 | 17.75 | 2251.1 | 25.54 | 2193 | 11.86 | 1808.4 | 24.91 | 105 | 2140 |
| cu10_10_38 | 0.13867 | 0.00158 | 0.27399 | 0.00401 | 5.23934 | 0.07458 | 0.03816 | 0.00105 | 0.972604 | 2210.6 | 19.69 | 1561 | 20.28 | 1859 | 12.14 | 756.9 | 20.51 | 71 | |
| cu10_10_22 | 0.13905 | 0.00175 | 0.38079 | 0.00592 | 7.30151 | 0.1112 | 0.04968 | 0.00126 | 0.979616 | 2215.4 | 21.64 | 2080 | 27.64 | 2149 | 13.6 | 979.9 | 24.2 | 94 | 2215 |
| cu10_10_33 | 0.14209 | 0.0015 | 0.34589 | 0.005 | 6.7774 | 0.09441 | 0.05813 | 0.00107 | 0.963658 | 2252.9 | 18.13 | 1914.9 | 23.97 | 2082.8 | 12.33 | 1142.1 | 20.48 | 85 | |
| cu10_10_13 | 0.14341 | 0.00208 | 0.39764 | 0.00612 | 7.85589 | 0.13028 | 0.07268 | 0.00139 | 0.928066 | 2268.8 | 24.73 | 2158.2 | 28.23 | 2214.6 | 14.94 | 1418.1 | 26.14 | 95 | 2269 |
| cu10_10_43 | 0.1447 | 0.00146 | 0.11153 | 0.00146 | 2.22497 | 0.02852 | 0.01453 | 0.00018 | 0.979184 | 2284.2 | 17.28 | 681.6 | 8.47 | 1188.9 | 8.98 | 291.5 | 3.59 | 30 | |
| cu10_10_32 | 0.14506 | 0.00144 | 0.26409 | 0.00349 | 5.28063 | 0.06746 | 0.06492 | 0.00079 | 0.96669 | 2288.5 | 16.94 | 1510.7 | 17.78 | 1865.7 | 10.91 | 1271.3 | 14.93 | 66 | |
| cu10_10_30 | 0.14534 | 0.00158 | 0.20693 | 0.003 | 4.14458 | 0.05891 | 0.0293 | 0.00043 | 0.980417 | 2291.7 | 18.56 | 1212.4 | 16.04 | 1663.1 | 11.63 | 583.8 | 8.44 | 53 | |
| cu10_10_08 | 0.14864 | 0.00174 | 0.16988 | 0.00233 | 3.48139 | 0.04898 | 0.04061 | 0.00053 | 0.974872 | 2330.3 | 19.96 | 1011.5 | 12.86 | 1523 | 11.1 | 804.6 | 10.27 | 43 | |
| cu10_10_19 | 0.15214 | 0.00157 | 0.20792 | 0.00292 | 4.36051 | 0.0592 | 0.02628 | 0.00031 | 0.966714 | 2370.1 | 17.45 | 1217.7 | 15.6 | 1704.9 | 11.21 | 524.3 | 6.02 | 51 | |
| cu10_10_39 | 0.15865 | 0.00219 | 0.4662 | 0.0071 | 10.19875 | 0.16135 | 0.06919 | 0.00137 | 0.96264 | 2441.3 | 23.14 | 2466.9 | 31.23 | 2453 | 14.63 | 1352.2 | 25.99 | 101 | 2441 |
| cu10_10_07 | 0.16209 | 0.00173 | 0.17636 | 0.00244 | 3.9405 | 0.05339 | 0.02703 | 0.0003 | 0.979307 | 2477.6 | 17.89 | 1047 | 13.36 | 1622 | 10.97 | 539.1 | 5.94 | 42 | |
| cu10_10_45 | 0.16354 | 0.00187 | 0.4792 | 0.0066 | 10.80397 | 0.15049 | 0.1026 | 0.00142 | 0.988787 | 2492.6 | 19.1 | 2523.8 | 28.75 | 2506.4 | 12.95 | 1974.2 | 26.03 | 101 | 2493 |
| cu10_10_29 | 0.16565 | 0.00243 | 0.4987 | 0.00787 | 11.38483 | 0.191 | 0.08355 | 0.00143 | 0.940651 | 2514.2 | 24.48 | 2608.2 | 33.83 | 2555.2 | 15.66 | 1621.9 | 26.74 | 104 | 2514 |
| cu10_10_44 | 0.16578 | 0.00213 | 0.48842 | 0.00714 | 11.16227 | 0.16921 | 0.0904 | 0.00173 | 0.964342 | 2515.5 | 21.48 | 2563.8 | 30.92 | 2536.8 | 14.13 | 1749.2 | 32.13 | 102 | 2516 |
| cu10_10_35 | 0.16675 | 0.00189 | 0.06249 | 0.00089 | 1.43701 | 0.02038 | 0.01663 | 0.00032 | 0.995783 | 2525.2 | 18.92 | 390.8 | 5.39 | 904.5 | 8.49 | 333.5 | 6.41 | 15 | |
| cu10_10_06 | 0.16697 | 0.0018 | 0.40846 | 0.00536 | 9.4033 | 0.12301 | 0.09854 | 0.00137 | 0.996885 | 2527.5 | 17.96 | 2207.9 | 24.52 | 2378.2 | 12.01 | 1899.6 | 25.2 | 87 | |
| cu10_10_03 | 0.16718 | 0.00176 | 0.30585 | 0.00395 | 7.04929 | 0.09035 | 0.04688 | 0.0006 | 0.992417 | 2529.6 | 17.56 | 1720.3 | 19.5 | 2117.7 | 11.4 | 926 | 11.52 | 68 | |

Table 2

| Spot | Pb207/Pb206 | ±1 | Pb206/U238 | ±1 | Pb207/U235 | ±1 | Pb208/Th232 | ±1 | Rho | Pb207/Pb206 | ±1 | Pb206/U238 | ±1 | Pb207/U235 | ±1 | Pb208/Th232 | ±1 | Conc. (%) | Age |
|---|---|---|---|---|---|---|---|---|---|---|---|---|---|---|---|---|---|---|---|
| cu10_10_24 | 0.16737 | 0.00173 | 0.46786 | 0.00644 | 10.79548 | 0.14426 | 0.10024 | 0.00124 | 0.97081 | 2531.5 | 17.24 | 2474.2 | 28.28 | 2505.7 | 12.42 | 1930.8 | 22.82 | 98 | 2532 |
| cu10_10_34 | 0.16818 | 0.00234 | 0.24908 | 0.0039 | 5.78027 | 0.0921 | 0.01957 | 0.00059 | 0.982685 | 2539.6 | 23.19 | 1433.7 | 20.15 | 1943.5 | 13.79 | 391.8 | 11.6 | 56 | |
| cu10_10_49 | 0.17622 | 0.00183 | 0.42874 | 0.006 | 10.4098 | 0.14184 | 0.06291 | 0.00114 | 0.973642 | 2617.6 | 17.21 | 2300 | 27.06 | 2471.9 | 12.62 | 1233.1 | 21.67 | 88 | |
| cu10_10_09 | 0.19711 | 0.00198 | 0.50672 | 0.00687 | 13.76983 | 0.1792 | 0.09987 | 0.00095 | 0.959888 | 2802.4 | 16.35 | 2642.6 | 29.38 | 2734 | 12.32 | 1924.1 | 17.38 | 94 | 2802 |
| cu10_10_36 | 0.22366 | 0.0022 | 0.62065 | 0.00826 | 19.13529 | 0.24394 | 0.07469 | 0.0017 | 0.957888 | 3007.3 | 15.75 | 3112.5 | 32.84 | 3048.7 | 12.3 | 1455.9 | 31.93 | 103 | 3007 |
| cu10_10_16 | 0.29784 | 0.00329 | 0.29915 | 0.00389 | 12.28395 | 0.15765 | 0.06696 | 0.00091 | 0.98695 | 3459 | 17.05 | 1687.1 | 19.29 | 2626.3 | 12.05 | 1310 | 17.18 | 49 | |

| CU10-19 | Isotope Ratios | | | | | | | | | Ages Ma | | | | | | | | Conc. (%) | Age |
|---|---|---|---|---|---|---|---|---|---|---|---|---|---|---|---|---|---|---|---|
| Spot | Pb207/Pb206 | ±1 | Pb206/U238 | ±1 | Pb207/U235 | ±1 | Pb208/Th232 | ±1 | Rho | Pb207/Pb206 | ±1 | Pb206/U238 | ±1 | Pb207/U235 | ±1 | Pb208/Th232 | ±1 | | |
| CU1019_21 | 0.0895 | 0.00103 | 0.06977 | 0.00113 | 0.86128 | 0.01429 | 0.02497 | 0.00042 | 0.976162 | 1414.9 | 21.85 | 434.8 | 6.82 | 630.8 | 7.8 | 498.4 | 8.21 | 31 | |
| CU1019_35 | 0.09193 | 0.00095 | 0.05095 | 0.00079 | 0.64582 | 0.01008 | 0.02045 | 0.00027 | 0.993422 | 1465.7 | 19.39 | 320.4 | 4.87 | 505.9 | 6.22 | 409.1 | 5.41 | 22 | |
| CU1019_23r | 0.09433 | 0.00108 | 0.05981 | 0.00096 | 0.77804 | 0.01281 | 0.01439 | 0.00022 | 0.974878 | 1514.7 | 21.48 | 374.5 | 5.85 | 584.4 | 7.32 | 288.7 | 4.38 | 25 | |
| CU1019_48 | 0.10777 | 0.00109 | 0.07755 | 0.00122 | 1.15216 | 0.01783 | 0.01536 | 0.0002 | 0.983695 | 1762 | 18.29 | 481.5 | 7.28 | 778.3 | 8.41 | 308 | 4.07 | 27 | |
| CU1019_07 | 0.10804 | 0.00128 | 0.0378 | 0.00059 | 0.56306 | 0.00923 | 0.0131 | 0.00018 | 0.952167 | 1766.5 | 21.58 | 239.2 | 3.7 | 453.5 | 6 | 263 | 3.58 | 14 | |
| CU1019_24 | 0.1136 | 0.00132 | 0.23388 | 0.00375 | 3.66411 | 0.06036 | 0.05233 | 0.00083 | 0.973324 | 1857.8 | 20.87 | 1354.8 | 19.61 | 1563.6 | 13.14 | 1030.9 | 16.03 | 73 | |
| CU1019_03 | 0.11389 | 0.00134 | 0.09842 | 0.00156 | 1.54539 | 0.02534 | 0.03554 | 0.00052 | 0.966658 | 1862.3 | 21.12 | 605.1 | 9.16 | 948.7 | 10.11 | 705.9 | 10.18 | 32 | |
| CU1019_37 | 0.11418 | 0.00117 | 0.13626 | 0.00212 | 2.14527 | 0.03346 | 0.03455 | 0.00049 | 0.997524 | 1867 | 18.45 | 823.5 | 12.04 | 1163.5 | 10.8 | 686.6 | 9.63 | 44 | |
| CU1019_06 | 0.11462 | 0.00128 | 0.12753 | 0.002 | 2.01547 | 0.03226 | 0.04167 | 0.00066 | 0.979782 | 1873.9 | 20.04 | 773.8 | 11.44 | 1120.7 | 10.86 | 825.2 | 12.74 | 41 | |
| CU1019_42 | 0.11531 | 0.00118 | 0.12033 | 0.00188 | 1.91271 | 0.02971 | 0.02426 | 0.00034 | 0.99419 | 1884.8 | 18.36 | 732.5 | 10.83 | 1085.5 | 10.36 | 484.5 | 6.8 | 39 | |
| CU1019_45 | 0.1156 | 0.0012 | 0.11539 | 0.00181 | 1.8388 | 0.02874 | 0.02272 | 0.00031 | 0.996419 | 1889.3 | 18.63 | 704 | 10.47 | 1059.4 | 10.28 | 454.1 | 6.2 | 37 | |
| CU1019_41 | 0.11622 | 0.00122 | 0.34145 | 0.00535 | 5.46987 | 0.08585 | 0.09278 | 0.00132 | 0.998305 | 1898.8 | 18.83 | 1893.6 | 25.73 | 1895.9 | 13.47 | 1793.3 | 24.49 | 100 | 1899 |
| CU1019_26 | 0.1163 | 0.0013 | 0.10778 | 0.00171 | 1.72835 | 0.0278 | 0.02735 | 0.00047 | 0.986381 | 1900.1 | 19.9 | 659.8 | 9.94 | 1019.1 | 10.35 | 545.4 | 9.24 | 35 | |
| CU1019_02 | 0.11729 | 0.0014 | 0.04682 | 0.00075 | 0.75722 | 0.0125 | 0.00979 | 0.00014 | 0.97038 | 1915.4 | 21.33 | 295 | 4.59 | 572.4 | 7.23 | 196.8 | 2.74 | 15 | |
| CU1019_20 | 0.11773 | 0.00159 | 0.34226 | 0.00572 | 5.55766 | 0.09929 | 0.08865 | 0.0015 | 0.935462 | 1922.1 | 24.06 | 1897.5 | 27.48 | 1909.6 | 15.37 | 1716.9 | 27.82 | 99 | 1922 |
| CU1019_44 | 0.11824 | 0.00122 | 0.13042 | 0.00204 | 2.12566 | 0.03307 | 0.02458 | 0.00035 | 0.994614 | 1929.7 | 18.31 | 790.3 | 11.65 | 1157.2 | 10.74 | 490.7 | 6.91 | 41 | |
| CU1019_22 | 0.11871 | 0.00147 | 0.02892 | 0.00047 | 0.47352 | 0.00805 | 0.00905 | 0.00014 | 0.955965 | 1936.9 | 22.01 | 183.8 | 2.96 | 393.6 | 5.55 | 182.1 | 2.88 | 9 | |
| CU1019_19 | 0.11894 | 0.00124 | 0.32024 | 0.00498 | 5.25142 | 0.08159 | 0.05405 | 0.00068 | 0.999094 | 1940.3 | 18.55 | 1790.9 | 24.32 | 1861 | 13.25 | 1064 | 13.1 | 92 | 1940 |
| CU1019_30 | 0.11896 | 0.00125 | 0.35066 | 0.0055 | 5.75176 | 0.09061 | 0.09525 | 0.00131 | 0.995637 | 1940.7 | 18.63 | 1937.8 | 26.27 | 1939.2 | 13.63 | 1838.9 | 24.2 | 100 | 1941 |
| CU1019_13 | 0.11934 | 0.00124 | 0.32203 | 0.00499 | 5.29858 | 0.08209 | 0.08141 | 0.00103 | 0.999831 | 1946.4 | 18.42 | 1799.6 | 24.36 | 1868.6 | 13.23 | 1582 | 19.23 | 92 | 1946 |
| CU1019_16 | 0.11958 | 0.00122 | 0.08706 | 0.00135 | 1.43532 | 0.02211 | 0.02358 | 0.00029 | 0.993402 | 1950 | 18.15 | 538.1 | 8 | 903.8 | 9.22 | 471.1 | 5.66 | 28 | |
| CU1019_05 | 0.12391 | 0.00146 | 0.08264 | 0.00131 | 1.41186 | 0.02306 | 0.01527 | 0.00022 | 0.97054 | 2013.2 | 20.72 | 511.9 | 7.78 | 893.9 | 9.71 | 306.3 | 4.47 | 25 | |
| CU1019_15 | 0.12502 | 0.00129 | 0.05309 | 0.00082 | 0.91507 | 0.01415 | 0.00835 | 0.0001 | 0.998847 | 2029.1 | 18.2 | 333.5 | 5.04 | 659.7 | 7.5 | 168 | 2.06 | 16 | |
| CU1019_27 | 0.13022 | 0.00147 | 0.09634 | 0.00152 | 1.72974 | 0.02785 | 0.02466 | 0.0004 | 0.979924 | 2100.9 | 19.67 | 592.9 | 8.97 | 1019.7 | 10.36 | 492.4 | 7.91 | 28 | |

Table 2

| Spot | Pb$^{207}$/Pb$^{206}$ | ±1 | Pb$^{206}$/U$^{238}$ | ±1 | Pb$^{207}$/U$^{235}$ | ±1 | Pb$^{208}$/Th$^{232}$ | ±1 | Rho | Pb$^{207}$/Pb$^{206}$ | ±1 | Pb$^{206}$/U$^{238}$ | ±1 | Pb$^{207}$/U$^{235}$ | ±1 | Pb$^{208}$/Th$^{232}$ | ±1 | Conc.(%) | Age |
|---|---|---|---|---|---|---|---|---|---|---|---|---|---|---|---|---|---|---|---|
| CU1019_14 | 0.13318 | 0.00136 | 0.21239 | 0.00329 | 3.89977 | 0.05998 | 0.06766 | 0.0009 | 0.9929 | 2140.2 | 17.68 | 1241.6 | 17.49 | 1613.6 | 12.43 | 1323.3 | 17.1 | 58 | |
| CU1019_09 | 0.13326 | 0.00144 | 0.10862 | 0.00169 | 1.99574 | 0.03141 | 0.01502 | 0.00021 | 0.988583 | 2141.4 | 18.8 | 664.7 | 9.83 | 1114.1 | 10.65 | 301.4 | 4.15 | 31 | |
| CU1019_29 | 0.13385 | 0.00138 | 0.08178 | 0.00128 | 1.50918 | 0.02362 | 0.00835 | 0.00011 | 0.999945 | 2149.1 | 17.9 | 506.7 | 7.64 | 934.1 | 9.56 | 168.1 | 2.24 | 24 | |
| CU1019_39 | 0.13402 | 0.00136 | 0.15571 | 0.00243 | 2.87636 | 0.04448 | 0.03107 | 0.00043 | 0.990904 | 2151.3 | 17.63 | 932.9 | 13.55 | 1375.7 | 11.65 | 618.5 | 8.48 | 43 | |
| CU1019_28 | 0.13806 | 0.00152 | 0.2056 | 0.00324 | 3.91333 | 0.06222 | 0.0783 | 0.00148 | 0.991148 | 2203 | 18.95 | 1205.3 | 17.31 | 1616.4 | 12.86 | 1523.8 | 27.8 | 55 | |
| CU1019_31 | 0.13818 | 0.00141 | 0.21007 | 0.00329 | 4.00241 | 0.06243 | 0.08532 | 0.00117 | 0.995955 | 2204.5 | 17.65 | 1229.2 | 17.51 | 1634.7 | 12.67 | 1654.9 | 21.79 | 56 | |
| CU1019_01 | 0.14111 | 0.00166 | 0.07446 | 0.00119 | 1.44858 | 0.02373 | 0.00488 | 0.00007 | 0.975593 | 2240.9 | 20.23 | 462.9 | 7.13 | 909.3 | 9.84 | 98.4 | 1.37 | 21 | |
| CU1019_11c | 0.14155 | 0.00145 | 0.07252 | 0.00112 | 1.41524 | 0.0218 | 0.00596 | 0.00007 | 0.997393 | 2246.3 | 17.6 | 451.3 | 6.75 | 895.4 | 9.17 | 120.1 | 1.49 | 20 | |
| CU1019_47 | 0.14206 | 0.00144 | 0.17947 | 0.00282 | 3.51453 | 0.05447 | 0.03766 | 0.00051 | 0.986354 | 2252.4 | 17.44 | 1064.1 | 15.4 | 1530.5 | 12.25 | 747.1 | 9.93 | 47 | |
| CU1019_25 | 0.147 | 0.00161 | 0.16646 | 0.00265 | 3.37436 | 0.05399 | 0.02413 | 0.00039 | 0.994979 | 2311.3 | 18.67 | 992.6 | 14.64 | 1498.5 | 12.53 | 481.9 | 7.67 | 43 | |
| CU1019_33 | 0.14976 | 0.00155 | 0.08052 | 0.00126 | 1.66273 | 0.02603 | 0.00725 | 0.0001 | 0.999573 | 2343.2 | 17.63 | 499.2 | 7.52 | 994.4 | 9.92 | 146 | 2 | 21 | |
| CU1019_40 | 0.15176 | 0.00155 | 0.20276 | 0.00317 | 4.24154 | 0.06577 | 0.04088 | 0.00055 | 0.991807 | 2365.9 | 17.36 | 1190.1 | 16.99 | 1682.1 | 12.74 | 809.9 | 10.76 | 50 | |
| CU1019_23c | 0.15741 | 0.00168 | 0.22776 | 0.00365 | 4.9443 | 0.07884 | 0.02888 | 0.00047 | 0.995008 | 2428 | 18.01 | 1322.8 | 19.14 | 1809.9 | 13.47 | 575.4 | 9.18 | 54 | |
| CU1019_43 | 0.15821 | 0.00161 | 0.27625 | 0.00432 | 6.02442 | 0.09322 | 0.02243 | 0.00032 | 0.989492 | 2436.6 | 17.09 | 1572.4 | 21.84 | 1979.4 | 13.48 | 448.4 | 6.33 | 65 | |
| CU1019_34 | 0.15946 | 0.00165 | 0.17697 | 0.00277 | 3.89103 | 0.06083 | 0.03194 | 0.00043 | 0.998788 | 2449.9 | 17.39 | 1050.4 | 15.16 | 1611.8 | 12.63 | 635.4 | 8.49 | 43 | |
| CU1019_18 | 0.16036 | 0.00162 | 0.20962 | 0.00325 | 4.63451 | 0.07112 | 0.03324 | 0.00043 | 0.989777 | 2459.4 | 16.99 | 1226.8 | 17.32 | 1755.5 | 12.82 | 660.9 | 8.37 | 50 | |
| CU1019_08 | 0.16323 | 0.00178 | 0.1431 | 0.00224 | 3.22063 | 0.05084 | 0.01956 | 0.00025 | 0.991616 | 2489.4 | 18.28 | 862.2 | 12.63 | 1462.1 | 12.23 | 391.5 | 4.99 | 35 | |
| CU1019_46 | 0.16328 | 0.00165 | 0.43629 | 0.00685 | 9.82044 | 0.15196 | 0.05802 | 0.0009 | 0.98556 | 2489.9 | 16.95 | 2334 | 30.73 | 2418.1 | 14.26 | 1139.9 | 17.27 | 94 | 2490 |
| CU1019_10 | 0.1634 | 0.00176 | 0.29667 | 0.00462 | 6.6835 | 0.10479 | 0.02073 | 0.00032 | 0.993236 | 2491.1 | 17.99 | 1674.8 | 22.96 | 2070.4 | 13.85 | 414.6 | 6.41 | 67 | |
| CU1019_17 | 0.16424 | 0.0017 | 0.37236 | 0.00579 | 8.4319 | 0.13037 | 0.09339 | 0.00115 | 0.994344 | 2499.8 | 17.27 | 2040.5 | 27.19 | 2278.6 | 14.03 | 1804.7 | 21.32 | 82 | |
| CU1019_38 | 0.16426 | 0.00174 | 0.42653 | 0.00668 | 9.66095 | 0.15218 | 0.10442 | 0.00144 | 0.994235 | 2500 | 17.7 | 2290 | 30.17 | 2403 | 14.49 | 2007.5 | 26.33 | 92 | 2500 |
| CU1019_11r | 0.16924 | 0.00171 | 0.19931 | 0.00308 | 4.65047 | 0.07136 | 0.0127 | 0.00016 | 0.992971 | 2550.1 | 16.87 | 1171.6 | 16.58 | 1758.4 | 12.82 | 255.1 | 3.18 | 46 | |
| CU1019_32 | 0.16942 | 0.00177 | 0.4596 | 0.00722 | 10.73659 | 0.16871 | 0.10597 | 0.00144 | 0.99973 | 2552 | 17.39 | 2437.8 | 31.87 | 2500.6 | 14.6 | 2035.9 | 26.31 | 96 | 2552 |
| CU1019_36 | 0.19988 | 0.00204 | 0.41896 | 0.00654 | 11.54677 | 0.17956 | 0.06458 | 0.0009 | 0.996194 | 2825.2 | 16.55 | 2255.8 | 29.7 | 2568.4 | 14.53 | 1265 | 17.08 | 80 | |
| CU1019_04 | 0.20072 | 0.00218 | 0.40989 | 0.00648 | 11.34428 | 0.17952 | 0.10204 | 0.00146 | 0.999014 | 2832.1 | 17.61 | 2214.4 | 29.64 | 2551.9 | 14.77 | 1964 | 26.79 | 78 | |
| CU1019_12 | 0.32842 | 0.00328 | 0.39916 | 0.00617 | 18.07325 | 0.27586 | 0.09508 | 0.00117 | 0.987448 | 3609.7 | 15.22 | 2165.1 | 28.44 | 2993.6 | 14.69 | 1835.8 | 21.63 | 60 | |

| CU10-21 | Isotope Ratios | | | | | | | | | Ages Ma | | | | | | | | Conc. (%) | Age |
|---|---|---|---|---|---|---|---|---|---|---|---|---|---|---|---|---|---|---|---|
| Spot | Pb$^{207}$/Pb$^{206}$ | ±1 | Pb$^{206}$/U$^{238}$ | ±1 | Pb$^{207}$/U$^{235}$ | ±1 | Pb$^{208}$/Th$^{232}$ | ±1 | Rho | Pb$^{207}$/Pb$^{206}$ | ±1 | Pb$^{206}$/U$^{238}$ | ±1 | Pb$^{207}$/U$^{235}$ | ±1 | Pb$^{208}$/Th$^{232}$ | ±1 | | |
| cu1021_04 | 0.05875 | 0.00184 | 0.05219 | 0.00082 | 0.42269 | 0.01318 | 0.01517 | 0.00034 | 0.503887 | 557.8 | 66.9 | 327.9 | 4.99 | 358 | 9.41 | 304.3 | 6.78 | 59 | |
| cu1021_19 | 0.05882 | 0.00103 | 0.06447 | 0.00089 | 0.52287 | 0.00983 | 0.01901 | 0.00029 | 0.734298 | 560.5 | 37.64 | 402.8 | 5.38 | 427.1 | 6.55 | 380.7 | 5.79 | 72 | |
| cu1021_18 | 0.05753 | 0.00083 | 0.06849 | 0.00091 | 0.5433 | 0.00882 | 0.0196 | 0.00028 | 0.818437 | 511.7 | 31.79 | 427.1 | 5.52 | 440.6 | 5.8 | 392.3 | 5.48 | 83 | |
| cu1021_01 | 0.0697 | 0.00081 | 0.15221 | 0.00198 | 1.46282 | 0.02028 | 0.04378 | 0.00054 | 0.938307 | 919.5 | 23.83 | 913.4 | 11.07 | 915.2 | 8.36 | 866 | 10.41 | 99 | 913 |

Table 2

| | | | | | | | | | | | | | | | | | | | |
|---|---|---|---|---|---|---|---|---|---|---|---|---|---|---|---|---|---|---|---|
| cu1021_20 | 0.09266 | 0.00109 | 0.14202 | 0.00205 | 1.81394 | 0.02689 | 0.01699 | 0.00027 | 0.973725 | 1480.8 | 22.28 | 856.1 | 11.56 | 1050.5 | 9.7 | 340.6 | 5.46 | 58 | 1481 |
| cu1021_15 | 0.09738 | 0.00106 | 0.16482 | 0.00224 | 2.21288 | 0.03072 | 0.03813 | 0.00044 | 0.978982 | 1574.5 | 20.29 | 983.5 | 12.42 | 1185.1 | 9.71 | 756.4 | 8.61 | 62 | |
| cu1021_14 | 0.10105 | 0.00113 | 0.16488 | 0.00229 | 2.2961 | 0.03263 | 0.03165 | 0.00038 | 0.97733 | 1643.6 | 20.56 | 983.8 | 12.68 | 1211.1 | 10.05 | 629.8 | 7.39 | 60 | |
| cu1021_10 | 0.10517 | 0.00116 | 0.288 | 0.0038 | 4.17457 | 0.0563 | 0.07772 | 0.00091 | 0.97835 | 1717.3 | 20.07 | 1631.5 | 19.02 | 1669 | 11.05 | 1512.8 | 17.1 | 95 | 1717 |
| cu1021_07 | 0.10526 | 0.00119 | 0.24328 | 0.00321 | 3.52977 | 0.04821 | 0.0532 | 0.00068 | 0.966068 | 1718.8 | 20.66 | 1403.7 | 16.62 | 1533.9 | 10.81 | 1047.7 | 12.97 | 82 | |
| cu1021_09 | 0.10527 | 0.00111 | 0.22882 | 0.00306 | 3.31999 | 0.04465 | 0.05278 | 0.00057 | 0.994358 | 1719 | 19.31 | 1328.3 | 16.03 | 1485.8 | 10.5 | 1039.5 | 10.88 | 77 | |
| cu1021_03 | 0.10565 | 0.00113 | 0.26981 | 0.00351 | 3.92999 | 0.05174 | 0.06086 | 0.00065 | 0.98813 | 1725.6 | 19.49 | 1539.8 | 17.82 | 1619.9 | 10.66 | 1194.1 | 12.4 | 89 | |
| cu1021_02 | 0.10611 | 0.00126 | 0.26828 | 0.00372 | 3.92285 | 0.05731 | 0.05635 | 0.00067 | 0.949131 | 1733.6 | 21.65 | 1532.1 | 18.9 | 1618.4 | 11.82 | 1108 | 12.91 | 88 | |
| cu1021_08 | 0.10672 | 0.00127 | 0.29082 | 0.00398 | 4.27817 | 0.06175 | 0.07516 | 0.00095 | 0.948156 | 1744.2 | 21.61 | 1645.6 | 19.88 | 1689.2 | 11.88 | 1464.7 | 17.87 | 94 | 1744 |
| cu1021_05 | 0.10706 | 0.00124 | 0.28383 | 0.00392 | 4.18779 | 0.06024 | 0.06454 | 0.00079 | 0.960125 | 1750 | 21.05 | 1610.6 | 19.66 | 1671.6 | 11.79 | 1264.2 | 15.04 | 92 | 1750 |
| cu1021_12 | 0.11056 | 0.00136 | 0.29142 | 0.0041 | 4.43991 | 0.06636 | 0.0642 | 0.00093 | 0.941309 | 1808.5 | 22.22 | 1648.6 | 20.46 | 1719.8 | 12.39 | 1257.6 | 17.72 | 91 | 1809 |
| cu1021_11 | 0.12546 | 0.00169 | 0.19809 | 0.00278 | 3.42549 | 0.05321 | 0.02949 | 0.00041 | 0.903466 | 2035.3 | 23.66 | 1165.1 | 14.95 | 1510.3 | 12.21 | 587.4 | 8.02 | 57 | |
| cu1021_06 | 0.17099 | 0.00182 | 0.45041 | 0.00592 | 10.61675 | 0.13961 | 0.10864 | 0.00128 | 0.999514 | 2567.4 | 17.71 | 2397.1 | 26.31 | 2490.2 | 12.2 | 2084.5 | 23.36 | 93 | 2567 |
| cu1021_13 | 0.19564 | 0.002 | 0.48771 | 0.00665 | 13.15517 | 0.17688 | 0.11554 | 0.00138 | 0.986103 | 2790.2 | 16.65 | 2560.7 | 28.8 | 2690.8 | 12.69 | 2209.9 | 25.04 | 92 | 2790 |
| cu1021_17 | 0.2171 | 0.00226 | 0.31304 | 0.0043 | 9.36954 | 0.12707 | 0.11033 | 0.00128 | 0.987316 | 2959.3 | 16.68 | 1755.7 | 21.1 | 2374.9 | 12.44 | 2115.3 | 23.39 | 59 | |
| cu1021_16 | 0.28685 | 0.00488 | 0.45133 | 0.00729 | 17.84857 | 0.31593 | 0.3418 | 0.00602 | 0.912527 | 3400.6 | 26.25 | 2401.2 | 32.38 | 2981.6 | 17.02 | 5942.7 | 90.61 | 71 | |

Table 2

| Analysis No. | Interf. Corr. Meth. | Total Hf beam (V) | $^{176}Hf/^{177}Hf$ | 2 se | exp. factor[1] | 2 se | $^{178}Hf/^{177}Hf$ | 2 se | $^{176}Yb/^{177}Hf$ | $^{176}Lu/^{177}Hf$ | Age (Ma) | $^{176}Hf/^{177}Hf$ Initial | 2 se | $e_{Hf}(t)$ | $T_{DM}$ (Ga) | $T_{DM}$ Crustal | $^{176}Hf/^{177}Hf$ corr. Using Hf corr. | 2 se |
|---|---|---|---|---|---|---|---|---|---|---|---|---|---|---|---|---|---|---|
| JM_Hf_01_15 | Yb | 7.7267499 | 0.2815469 | 4.37E-05 | 1.020608 | 0.005 | 1.4672422 | 7E-05 | 0.0791438 | 0.001265 | 2502 | 0.281487 | 1.53 | 10.68 | 2.4043437 | 2.34182005 | 0.2815971 | 2.6362E-05 |
| JM_Hf_01_30 | Yb | 6.97000027 | 0.2814981 | 3.97E-05 | 0.982525 | 0.004 | 1.4671924 | 8E-05 | 0.1199486 | 0.0018417 | 2536 | 0.281409 | 1.389 | 8.71 | 2.5097703 | 2.49532256 | 0.2816157 | 2.4981E-05 |
| JM_Hf_01_33 | Yb | 4.67409563 | 0.2817055 | 6.73E-05 | 1.014573 | 0.01 | 1.4674114 | 1E-04 | 0.1164454 | 0.0019953 | 2582 | 0.281607 | 2.356 | 16.82 | 2.2278493 | 2.00494879 | 0.2817055 | 3.5205E-05 |
| JM_Hf_01_37 | Yb | 8.56295776 | 0.2815566 | 3.19E-05 | 1.020134 | 0.004 | 1.4672625 | 7E-05 | 0.0697596 | 0.0010969 | 2524 | 0.281504 | 1.117 | 11.82 | 2.380387 | 2.28583914 | 0.281586 | 2.0288E-05 |
| JM_Hf_01_38 | Yb | 7.40262413 | 0.2812862 | 3.25E-05 | 1.033512 | 0.005 | 1.4673431 | 7E-05 | 0.0470695 | 0.0008719 | 2535 | 0.281244 | 1.138 | 2.82 | 2.7348851 | 2.87300711 | 0.2813529 | 2.1851E-05 |
| JM_Hf_01_45 | Yb | 6.45147038 | 0.2817449 | 4.89E-05 | 1.040761 | 0.004 | 1.4672911 | 6E-05 | 0.1125767 | 0.0021122 | 2579 | 0.281641 | 1.711 | 17.94 | 2.179038 | 1.92923966 | 0.281856 | 2.9142E-05 |
| JM_Hf_01_46 | Yb | 6.88419962 | 0.2814017 | 2.67E-05 | 1.054967 | 0.003 | 1.4672855 | 5E-05 | 0.0868036 | 0.0013939 | 2588 | 0.281333 | 0.933 | 7.20 | 2.6132661 | 2.63247957 | 0.2814606 | 1.7329E-05 |
| JM_Hf_19_13 | Yb | 6.51400232 | 0.2818783 | 4.57E-05 | 0.946077 | 0.004 | 1.4672898 | 7E-05 | 0.1250521 | 0.0019712 | 1946 | 0.281805 | 1.598 | 9.26 | 1.981933 | 2.00603938 | 0.2819746 | 2.5521E-05 |
| JM_Hf_19_19 | Yb | 6.74017954 | 0.2817528 | 3.98E-05 | 1.020251 | 0.004 | 1.467259 | 6E-05 | 0.1095165 | 0.0016014 | 1940 | 0.281694 | 1.393 | 5.16 | 2.1383087 | 2.26506384 | 0.2818477 | 2.3284E-05 |
| JM_Hf_19_20 | Yb | 5.80164814 | 0.2818532 | 4.61E-05 | 0.952946 | 0.004 | 1.4672763 | 7E-05 | 0.1482728 | 0.002333 | 1922 | 0.281768 | 1.614 | 7.38 | 2.0374081 | 2.10847924 | 0.2820193 | 2.8992E-05 |
| JM_Hf_19_30 | Yb | 6.37135839 | 0.2818805 | 4.61E-05 | 0.900548 | 0.004 | 1.4673305 | 7E-05 | 0.1376463 | 0.0021143 | 1941 | 0.281803 | 1.615 | 9.03 | 1.9864736 | 2.016565 | 0.2820187 | 2.7215E-05 |
| JM_Hf_19_32 | Yb | 6.26128387 | 0.2812917 | 3.23E-05 | 0.911954 | 0.004 | 1.4672649 | 7E-05 | 0.0366123 | 0.0006812 | 2552 | 0.281259 | 1.13 | 3.73 | 2.7139516 | 2.82777192 | 0.2813285 | 2.0609E-05 |
| JM_Hf_19_38 | Yb | 6.36559486 | 0.2812602 | 3.59E-05 | 0.892199 | 0.004 | 1.4672655 | 6E-05 | 0.0571406 | 0.0009523 | 2500 | 0.281215 | 1.256 | 0.97 | 2.7759337 | 2.96413081 | 0.2813367 | 2.4456E-05 |
| JM_Hf_19_41 | Yb | 6.302877 | 0.2817551 | 3.66E-05 | 0.884152 | 0.004 | 1.4672875 | 6E-05 | 0.1334779 | 0.0020305 | 1899 | 0.281682 | 1.279 | 3.79 | 2.1597813 | 2.32070425 | 0.28187 | 2.0887E-05 |
| JM_Hf_19_46 | Yb | 7.23973465 | 0.2817371 | 3.85E-05 | 0.859876 | 0.004 | 1.4672395 | 7E-05 | 0.1154007 | 0.0017602 | 2490 | 0.281653 | 1.346 | 16.34 | 2.1695293 | 1.96572306 | 0.2817581 | 2.4025E-05 |

Table 3

81

| Sample | Sample Mass | d13C (‰) | d18O (‰) |
|---|---|---|---|
| T2<br>(15º33'39.4"N, 78º10'17.9"E) | 124ug | -1.5449 | -16.8622 |
| T1<br>(15º33'39.4"N, 78º10'17.9"E) | 91ug | 0.2553 | -17.0593 |
| V1<br>(15º30'38.4"N, 18º10'17.5"E) | 134ug | 1.4502 | -6.8339 |

Table 4